Mon. Not. R. Astron. Soc. **000**, 1–31 (2007) Printed 1 February 2008 (MN LATEX style file v2.2)

Horizon-Penetrating Transonic Accretion Disks around Rotating Black Holes

Rohta Takahashi[1⋆]
[1] *Graduate School of Arts and Sciences, University of Tokyo, Komaba, Meguro, Tokyo 153-8902, Japan*

Accepted 200X December 15. Received 200X December 14; in original form 200X October 11

ABSTRACT

The stationary hydrodynamic equations for the transonic accretion disks and flows around rotating black holes are presented by using the Kerr-Schild coordinate where there is no coordinate singularity at the event horizon. We use two types of the causal viscosity prescription, and the boundary conditions for the transonic accretion flows are given at the sonic point. For one type of the causal viscosity prescription we also add the boundary conditions at the viscous point where the accreting radial velocity is nearly equal to the viscous diffusion velocity. Based on the formalism for the transonic accretion disks, after we present the calculation method of the transonic solutions, the horizon-penetrating transonic solutions which smoothly pass the event horizon are calculated for several types of the accretion flow models: the ideal isothermal flows, the ideal and the viscous polytropic flows, the advection dominated accretion flows (ADAFs) with the relativistic equation of state, the adiabatic accretion disks, the standard accretion disks, the supercritical accretion disks. These solutions are obtained for both non-rotating and rotating black holes. The calculated accretion flows plunge into black hole with finite three velocity smaller than the speed of light even at the event horizon or inside the horizon, and the angular velocities of the accretion flow at the horizon are generally different from the angular velocity of the frame-dragging due to the black hole's rotation. These features contrast to the results obtained by using the Boyer-Lindquist coordinate with the coordinate singularity at the horizon.

Key words: accretion: accretion disks—black holes—Galaxy: center.

1 INTRODUCTION

Elucidating the nature of the strong-gravity region around a black hole is one of the greatest challenges in astrophysics in this century. The most of the gravitational energy is converted into another forms of energies such as the kinetic, the thermal and/or the radiation energy, and especially the emission from the vicinity of the event horizon contains information about physics of the strong-gravity region such as the physical parameters of a black hole. Since such emission by e.g. photons or neutrinos is usually produced in the accretion flows plunging into the black hole, the structure of the accretion flows in the vicinity of the black hole's horizon is frequently required to be solved precisely. Especially, the effects of the frame dragging due to the black hole's rotation are taken into account only when the fully general relativistic calculations are done.

In the past studies, for many astrophysical systems and situations, the stationary solutions for the structure of the transonic accretion flows near the horizon are solved for the standard accretion disks (Novikov & Thorne 1973; Page & Thorne 1974), the advection-dominated accretion flows (Chakrabarti 1996; Abramowicz et al. 1997; Jaroszyski & Kurpiewski 1997; Gammie & Popham 1998; Popham & Gammie 1998; Manmoto 2000), the polytropic accretion flows (Peitz & Appl 1997), the super-critical accretion flows (Beloborodov 1998; Shimura & Manmoto 2003), and the hypercritical accretion flow model for the neutrino-dominated accretion flow (Popham, Woosley & Fryer 1999). All these works use the Boyer-Lindquist coordinate where the coordinate singularity exists at the horizon. Due to the coordinate singularity, some physical values of the accretion flow based on the calculations using the Boyer-Lindquist coordinate are not realistic. For example, the radial component of

⋆ E-mail: rohta@ea.c.u-tokyo.ac.jp

three velocity of the accretion flow equals to the speed of light at the horizon, and the corresponding gamma factor diverges just outside the horizon. But these features are not the cases for the realistic accretion flow, i.e., the accretion flows plunge into the horizon with some finite velocity smaller than the speed of light, because from the point of view of the local observer moving along the fluid motion, the horizon is not a special location. So, one of the possible natural next step is to extend these past studies to the formulation using the Kerr-Schild coordinate where there is no coordinate singularity at the horizon. Our calculations in this study by using the Kerr-Schild coordinate avoiding the coordinate singularity show the radial velocity smaller than the speed of light at the horizon. In this study, we first show all the explicit formulation for the transonic accretion flows written by the Kerr-Schild coordinate, and then calculate the horizon-penetrating transonic solutions for the accretion flow which do not have any singularity at the horizon.

The Kerr-Schild coordinates are frequently used in the past study, especially for the dynamical numerical calculations of the hydrodynamics or the magnetohydrodynamics around the black holes (Papadopoulos & Font 1998; Font, Ibáñez & Papadopoulos 1998; Cook 2000; Font 2000; Komissarov 2001; Gammie, McKinney & Tóth 2003; Komissarov 2004; Gammie, Shapiro & McKinney 2004). While these studies mainly concentrate on the dynamical calculations of the accretion flows around the black hole, Papadopoulos & Font (1998) also give the simple solutions for the stationary accretion flows plunging into the black hole which exhibit the maximum value of the radial speed at the horizon. In our calculations, we found that this feature is not a general statement in the viscous accretion flows, i.e., the maximum value of the radial velocity is not generally achieved at the position of the horizon.

In the present study, we concentrate on the stationary axisymmetric accretion flow in the equatorial plane. In this study, we use two types of the causal viscosity prescription. One is the simple treatment of the kinematic viscosity so as to vanish the shear stress at the horizon. The other is based on the description of the shear stress measured in the fluid's rest frame. The latter type of the causal viscosity is considered by Papaloizou & Szuszkiewicz (1994) for the Newtonian case and Gammie & Popham (1998) for the relativistic case. By using the latter types of the causal viscosity prescription, we do not need to put the boundary condition on the horizon, such as zero-boundary condition used in, e.g., Narayan, Kato & Honma (1997). In this study, we give the formulation with the effects of the heat flux (or the radiation cooling), the heat inertia and the relativistic enthalpy, and the relatively general forms of the equation of state. Based on this formalism, we give the sample transonic solutions for three types of accretion flow models: ideal isothermal disks, polytropic disks and advection-dominated accretion flows (ADAFs) with the relativistic equation of state, the adiabatic accretion disks, the standard accretion disks, and the supercritical accretion disks.

We give the preliminaries for the calculations of the transonic solutions by using the Kerr-Schild coordinate in §2 containing such as the background metric and the frame and the frame transformation used in this study. In §3, the basic equations are given; the mass conservation (§3.1), the radial momentum equation (§3.2), the angular momentum equation (§3.3), the equation for vertical structure which is the momentum conservation in θ-direction (§3.4), the thermodynamic equation and the energy equation (§3.5), the turbulent shear stress based on the causal viscosity (§3.6). The boundary conditions for the viscous transonic solutions are given in §4; the boundary conditions at the sonic point (§4.1) and the viscous point (§4.2). In §5, we summarize the coupled differential equations to be solved. We give the calculation procedures in §6. Formulation and/or Numerical solutions for the horizon-penetrating solutions of the transonic accretion flows for different types of the accretion flow models are presented in §7: the formulation and the numerical solutions for the ideal isothermal accretion flow (§7.1), the polytropic disks (§7.2), the ADAF with relativistic equation of state (§7.3), the adiabatic accretion disk and the standard accretion disk (§7.4), the formulation for the supercritical accretion disk (§7.5). We give concluding remarks in the last section. While the basic structure of the basic equations for the transonic accretion flows are simple, the explicit expressions for some formula are lengthy. In order to clearly see the outline of the calculations, we put the details of lengthy formula in the Appendix and in the main body only the important formula are given.

2 METRIC, REFERENCE FRAME AND VELOCITY FIELDS

2.1 Background Metric

Throughout the present study, we assume the background geometry around the rotating black hole written by the Kerr-Schild coordinate described as

$$ds^2 = -\alpha^2 dt^2 + \gamma_{ij}(dx^i + \beta^i dt)(dx^j + \beta^j dt), \tag{1}$$

where $i,\ j = r,\ \theta,\ \phi$, and the nonzero components of the lapse function α, the shift vector β^i and the spatial matrix γ_{ij} are given in the geometric units as

$$\begin{aligned} \alpha &= \left(1+\frac{2mr}{\Sigma}\right)^{-1/2},\ \beta^r = \frac{2mr/\Sigma}{1+2mr/\Sigma}, \\ \gamma_{rr} &= 1+\frac{2mr}{\Sigma}, \gamma_{\theta\theta} = \Sigma,\ \ \gamma_{\phi\phi} = \frac{A\sin^2\theta}{\Sigma}, \gamma_{r\phi} = \gamma_{\phi r} = -a\sin^2\theta\left(1+\frac{2mr}{\Sigma}\right). \end{aligned} \tag{2}$$

Here, we use the geometric mass $m = GM/c^2$, $\Sigma = r^2 + a^2\cos^2\theta$, $\Delta = r^2 - 2Mr + a^2$ and $A = (r^2+a^2)^2 - a^2\Delta\sin^2\theta$, where M is the black hole mass, G is the gravitational constant and c is the speed of light. Explicit forms of nonzero components of metric $g_{\mu\nu}$ and its inverse $g^{\mu\nu}$ are calculated in Appendix A. The position of the outer and inner horizon, $r_\pm$, is calculated from $\Delta = 0$ as $r_\pm = m \pm (m^2 - a^2)^{1/2}$. The angular velocity of the frame dragging due to the black hole's rotation is calculated as $\omega = -g_{t\phi}/g_{\phi\phi} = 2mar/A$. Although some past studies use the metric in the equatorial plane, i.e. $\theta = \pi/2$, we basically formulate the basic equations by using the metric including θ. This is because in the calculations of the vertical structure of the accretion disk which are performed in Sec. 3.4 and Appendix F need the metric including θ, and we would like to have the consistency of the notation of the metric throughout the paper. But, we actually calculate the transonic solutions of the accretion flow in Sec.7 by setting $\theta = \pi/2$.

2.2 Reference Frames

In this study, we use three types of reference frames. The first is the Kerr-Schild coordinate frame (KSF), in which most of our calculations are done. The second is the fluid's rest frame (FRF), an orthonormal tetrad basis carried by observers moving along the fluid. The components of the four velocity measured in the FRF are described as

$$u^{(t)} = -u_{(t)} = 1, \quad u^{(i)} = u_{(i)} = 0, \quad (i = r,\ \theta,\ \phi) \tag{3}$$

where the bracket denote the physical quantities measured in the FRF. The third frames are calculated from a stationary congruences formed by observers with a future-directed unit vector orthogonal to t =constant whose components are given as

$$u_t = -\alpha, \quad u_i = 0, \quad (i = r,\ \theta,\ \phi), \tag{4}$$

and

$$u^t = \alpha^{-1}, \quad u^i = -\alpha^{-1}\beta^i, \quad (i = r,\ \theta,\ \phi), \tag{5}$$

respectively. For this congruences, since the vorticity tensor vanishes [e.g., A.10.2 in Frolov & Novikov (1998)], this congruences is the congruences of locally non-rotating observers. So, this frame is usually called as the locally non-rotating reference frame (LNRF). By using the Boyer-Lindquist coordinate, this observer is moving with the angular velocity of the frame-dragging due to the black hole's rotation (Bardeen 1970; Bardeen, Press & Teukolsky 1972). On the other hand, by using the Kerr-Schild coordinate, since $\beta^r \neq 0$ and $\beta^\theta = \beta^\phi = 0$, the observers with $u_\mu = -\alpha\delta^t_\mu$ is radially falling with $u^\theta = u^\phi = 0$. For such observers, the nonzero components of the covariant and the contravariant four velocities are given as

$$u_t^{\rm LNRF} = -\alpha, \quad u^t_{\rm LNRF} = \frac{1}{\alpha}, \quad u^r_{\rm LNRF} = -\frac{\beta^r}{\alpha}. \tag{6}$$

We can easily show that the LNRF is an orthonormal tetrad basis carried by the observer moving with $u^\mu_{\rm LNRF}$. The physical quantities measured in the LNRF are described by using the hat such as $u^{\hat\mu}$, $u_{\hat\mu}$, etc. In the Kerr-Schild coordinate, since the congruences of the observers moving with the angular velocity of the frame-dragging have the singularity at the event horizon as shown in the Appendix B, we do not use such congruences in our calculations.

2.3 Frame Transformations and Velocity Fields

The physical quantities measured in the KSF are transformed to those in the LNRF by tetrads $e_\mu{}^{\hat\nu}$ and $e^\mu{}_{\hat\nu}$. For example, the four velocity is transformed as $u^\mu = e^\mu{}_{\hat\nu} u^{\hat\nu}$ and $u_\mu = e_\mu{}^{\hat\nu} u_{\hat\nu}$. The explicit expressions of the tetrad components $e_\mu{}^{\hat\nu}$ and $e^\mu{}_{\hat\nu}$ are given in Appendix C.

The FRF usually moves with some radial and azimuthal velocities with respect to the LNRF. We newly defined the radial velocity v_r and the rotational velocity $\hat v_\phi$ such that the FRF moves with the radial velocity v_r and the azimuthal velocity $\hat v_\phi$ with respect to the LNRF. By using these velocities, the physical quantities in the LNRF are transformed to those in the FRF by two-dimensional Lorentz transformation $e_{\hat\nu}{}^{(\lambda)}$ and $e^{\hat\nu}{}_{(\lambda)}$ with the radial velocity v_r and the azimuthal velocity $\hat v_\phi$. Here, $e_{\hat\nu}{}^{(\lambda)}$ and $e^{\hat\nu}{}_{(\lambda)}$ are the transformation matrices denoting the two-dimensional Lorentz transformations, and the explicit expressions of these matrices are also given in Appendix C.

By using the tetrads described in Appendix C, all the covariant and contravariant components of the four velocity in the KSF are calculated as $u^\mu = e^\mu{}_{\hat\alpha} e^{\hat\alpha}{}_{(\nu)} u^{(\nu)}$ and $u_\mu = e_\mu{}^{\hat\alpha} e_{\hat\alpha}{}^{(\nu)} u_{(\nu)}$, and described by using the radial velocity $\hat v_r$ and the azimuthal velocity $\hat v_\phi$ of the FRF measured in the LNRF as shown in Appendix D. Inversely, the radial velocity $\hat v_r$ and the azimuthal velocity $\hat v_\phi$ are described by the four velocities, u^μ and u_μ, measured in the KSF as

$$\hat v_r = \frac{u^r + \beta^r u^t}{\hat\gamma(\gamma_{rr})^{1/2}}, \quad \hat v_\phi = \frac{\ell}{\hat\gamma(\gamma_{\phi\phi})^{1/2}}, \tag{7}$$

where $\hat\gamma \equiv (1 - \hat v_r^2 - \hat v_\phi^2)^{-1/2} = \alpha u^t$. Since $\hat v_r$ is the radial velocity measured in the LNRF which is radially falling with $u^r_{\rm LNRF}$, the radial velocity $\hat v_r$ can generally have both the positive and the negative values for the radially falling accretion flows.

2.4 u^t and Ω

When the transonic solutions are calculated later, we solve the differential equations for the radial four velocity u^r and the angular momentum $\ell(=u_\phi)$. Therefore, it is convenient to express the angular velocity Ω and u^t which are frequently used in the formula in the following sections by u^r and ℓ. From the normalization of the four velocity, $u^\mu u_\mu = -1$, we can obtain the quadratic equation of u^t as $A_0(u^t)^2 + 2B_0 u^t + C_0 = 0$ where $A_0 = -\alpha^2 + (\beta^r)^2/\gamma^{rr}$, $B_0 = (\beta^r/\gamma^{rr})u^r$ and $C_0 = (u^r)^2/\gamma^{rr} + \ell^2/\gamma_{\phi\phi} + 1$. From the quadratic equation, we have the solution for $u^t > 0$ as

$$u^t = \frac{C_0}{D_0^{1/2} - B_0}, \tag{8}$$

where $D_0 = B_0^2 - A_0 C_0$. In this study, we consider the accretion flow with $u^r < 0$. For such flows, $B_0 < 0$, and then $u^t > 0$. We can also show that $D_0 > 0$ for the region $r > r_+$, and for the region $r < r_0$, $D_0 > 0$ only when $\ell^2 < [(u^r)^2 + 1/\Sigma]A/(-\Delta)$. From u^t calculated above, the angular velocity Ω is calculated as

$$\Omega = \omega + \frac{\ell - \gamma_{r\phi}u^r}{u^t \gamma_{\phi\phi}} \tag{9}$$

which is derived from $\ell = g_{\phi\mu}u^\mu$. Here, u^t is calculated from Eq. (8). We can also calculate u_r and $\mathcal{E}(\equiv -u_t)$ from u^r and ℓ as $u_r = (g_{tr} + g_{r\phi}\Omega)u^t + g_{rr}u^r$ and $\mathcal{E} = (g_{tt} + g_{t\phi}\Omega)u^t + g_{tr}u^r$ where u^t and Ω are calculated by Eqs. (8) and (9).

2.5 Transformation of Four Velocities written by Kerr-Schild Coordinate and Boyer-Lindquist Coordinate

The transformation of the four velocities calculated by using the Boyer-Lindquist coordinate and the Kerr-Schild coordinate are given by

$$u^t_{\rm BL} = u^t_{\rm KS} - \frac{2mr}{\Delta}u^r_{\rm KS}, \quad u^r_{\rm BL} = u^r_{\rm KS}, \quad u^\theta_{\rm BL} = u^\theta_{\rm KS}, \quad u^\phi_{\rm BL} = u^\phi_{\rm KS} - \frac{a}{\Delta}u^r_{\rm KS}, \tag{10}$$

$$u_t^{\rm BL} = u_t^{\rm KS}, \quad u_r^{\rm BL} = u_r^{\rm KS} + \frac{2mr}{\Delta}u_t^{\rm KS} + \frac{a}{\Delta}u_\phi^{\rm KS}, \quad u_\theta^{\rm BL} = u_\theta^{\rm KS}, \quad u_\phi^{\rm BL} = u_\phi^{\rm KS}. \tag{11}$$

Here, "BL" and "KS" denote the physical quantities calculated by using the Boyer-Lindquist coordinate and the Kerr-Schild coordinate, respectively. [1]

3 BASIC EQUATIONS

The basic equations for the relativistic hydrodynamics are the baryon-mass conservation $(\rho_0 u^\mu)_{;\mu} = 0$ and the energy-momentum conservation $T^{\mu\nu}_{\ ;\nu} = 0$, where ρ_0 is the rest-mass density and $T^{\mu\nu}$ is the energy-momentum tensor. Dynamical basic equations except the baryon mass conservation are calculated from the energy-momentum tensor, $T^{\mu\nu}$. We use the energy-momentum tensor written as,

$$T^{\mu\nu} = \rho_0 \eta u^\mu u^\nu + p g^{\mu\nu} + t^{\mu\nu} + q^\mu u^\nu + q^\nu u^\mu, \tag{12}$$

where p is the pressure, $\eta = (\rho_0 + u + p)/\rho_0$ is the relativistic enthalpy, u is the internal energy, $t^{\mu\nu}$ is the viscous stress-energy tensor and q^μ is the heat-flux four vector. In the present study, we do not include the heat flux term in the energy-momentum tensor.

One of the natural form of the shear stress, $t^{\mu\nu}$, is the Navier-Stokes shear stress. The relativistic Navier-Stokes shear stress, $t^{\mu\nu}$, is written as (Misner, Thorne & Wheeler 1973),

$$t^{\mu\nu} = -2\lambda\sigma^{\mu\nu} - \zeta\Theta h^{\mu\nu}, \tag{13}$$

[1] The transformation law given by Eq. (10) is calculated from the lapse function α, the shift vector β^μ (or β_μ) and the matrix γ_{ij} (or γ^{ij}) for the Kerr-Schild coordinate as

$$u^t_{\rm BL} = u^t_{\rm KS} - \frac{\beta^r}{\alpha^2\gamma^{rr} - (\beta^r)^2}u^r_{\rm KS}, \qquad u^\phi_{\rm BL} = u^\phi_{\rm KS} + \left(\frac{\gamma_{r\phi}}{\gamma_{\phi\phi}}\right)\frac{\alpha^2\gamma^{rr}}{\alpha^2\gamma^{rr} - (\beta^r)^2}u^r_{\rm KS},$$

which are derived from the metric expressed as

$$\begin{aligned} ds^2 &= -\frac{\alpha^2\gamma^{rr} - (\beta^r)^2}{\gamma^{rr}}\left[dt - \frac{\beta^r}{\alpha^2\gamma^{rr} - (\beta^r)^2}dr\right]^2 + \left[\frac{\alpha^2}{\alpha^2\gamma^{rr} - (\beta^r)^2}\right]dr^2 + \gamma_{\theta\theta}d\theta^2 \\ &\quad + \gamma_{\phi\phi}\left\{d\phi + \left(\frac{\gamma_{r\phi}}{\gamma_{\phi\phi}}\right)\frac{\alpha^2\gamma^{rr}}{\alpha^2\gamma^{rr} - (\beta^r)^2}dr + \beta^r\left(\frac{\gamma_{r\phi}}{\gamma_{\phi\phi}}\right)\left[dt - \frac{\beta^r}{\alpha^2\gamma^{rr} - (\beta^r)^2}dr\right]\right\}^2 \end{aligned}$$

where λ is the coefficient of dynamic viscosity, ξ is the coefficient of bulk viscosity, $h^{\mu\nu} \equiv g^{\mu\nu} + u^\mu u^\nu$ is the projection tensor, $\Theta \equiv u^\gamma{}_{;\gamma}$ is the expansion of the fluid world line, and $\sigma^{\mu\nu}$ is the shear rate of the fluid which is calculated as

$$\sigma_{\mu\nu} = \frac{1}{2}(u_{\mu;\alpha}h^\alpha_\nu + u_{\nu;\alpha}h^\alpha_\mu) - \frac{1}{3}\Theta h_{\mu\nu}, \tag{14}$$

$$= \frac{1}{2}(u_{\mu;\nu} + u_{\nu;\mu} + a_\mu u_\nu + a_\nu u_\mu) - \frac{1}{3}\Theta h_{\mu\nu}, \tag{15}$$

where $a_\mu \equiv u_{\mu;\gamma}u^\gamma$ is the four acceleration. In this study, we do not take the shear stress written by this form. Instead, we use the Kerr-Schild coordinate version of the shear stress used in Gammie & Popham (1998) and Popham & Gammie (1998) which allows angular momentum transport and preserve causality. We evaluate the shear stress in the FRF and assume that all the components of the shear stress except $t_{(r)(\phi)} = t_{(\phi)(r)}$ are null in the FRF. Based on this assumption, the shear stress measured in the KSF is calculated by using the tetrads connecting the KSF and the FRF, e.g., $t^\mu{}_\nu = 2[e^{\mu(r)}e_\nu{}^{(\phi)} + e^{\mu(\phi)}e_\nu{}^{(r)}]\ t_{(r)(\phi)}$. The explicit forms of the shear stress in the FRF used in this study is given in Sec. 3.6.

In this study, we consider the stationary, axisymmetric and equatorially symmetric global accretion flow in the equatorial plane, i.e., we assume $u_\theta = 0$. We also assume that the effects of the bulk viscosity is negligible. In the following sections, we derive the basic equations written by the Kerr-Schild coordinate by using the vertical averaging procedures used in, e.g., Gammie & Popham (1998), around the equatorial plane.

3.1 Mass Conservation and Mass-Energy Flux

The equation for the baryon mass conservation is written as

$$(\rho_0 u^\mu)_{;\mu} = 0, \tag{16}$$

where ρ_0 is the rest-mass density and u^μ is the four velocity. By averaging the physical quantities around the equatorial plane, the mass-accretion rate $\dot{M}$ is calculated as

$$\dot{M} = -4\pi\sqrt{-g}H_\theta \rho_0 u^r, \tag{17}$$

where H_θ is the half-thickness of the accretion flow in the θ-direction which is calculated in Sec. 3.4, and $\sqrt{-g} = r^2$. When we calculate the global structure of the accretion flow, we normalize the rest-mass density, ρ_0, by setting $\dot{M} = 1$, i.e., the mass conservation is written as

$$-4\pi r^2 H_\theta \rho_0 u^r = 1. \tag{18}$$

From the projection of the energy-momentum conservation, $T^{\mu\nu}_{\ \ ;\nu} = 0$, onto t-component, i.e., $h^t_\mu T^{\mu\nu}_{\ \ ;\nu} = 0$, with the vertical averaging calculations, we get

$$\left[\eta\mathcal{E} + \frac{4\pi H_\theta\sqrt{-g}}{\dot{M}}(t^r{}_t + u^r q_t - q^r\mathcal{E})\right]_{,r} = \frac{4\pi H_\theta\sqrt{-g}}{\dot{M}}\mathcal{E}q^\theta. \tag{19}$$

From Eq. (19), we obtain

$$\eta\mathcal{E} - \epsilon_0 + \frac{4\pi H_\theta\sqrt{-g}}{\dot{M}}t^r{}_t = Q_\mathcal{E}, \tag{20}$$

where ϵ_0 is the specific energy of the flow and $Q_\mathcal{E}$ represents the effects of the heat flux defined as

$$Q_\mathcal{E} \equiv \int_{r_{\rm min}}^{r_{\rm max}} \frac{4\pi H_\theta\sqrt{-g}}{\dot{M}}\mathcal{E}q^\theta dr - \frac{4\pi H_\theta\sqrt{-g}}{\dot{M}}\left(u^r q_t - q^r\mathcal{E}\right). \tag{21}$$

In the case of no heat flux, Eq. (19) is reduced to

$$\dot{E} = \dot{M}\eta\mathcal{E} + 4\pi r^2 H_\theta t^r{}_t, \tag{22}$$

where $\dot{E}$ is the mass-energy flux corresponding to the rate of change of the black hole mass if measured at the horizon. With the mass conservation, we obtain the specific energy ϵ_0 as

$$\epsilon_0 = \frac{\dot{E}}{\dot{M}} = \eta\mathcal{E} + \frac{t^r{}_t}{\rho_0 u^r}, \tag{23}$$

where ϵ_0 is the specific energy of the accreting matter. When the velocity of the accreting matter is non-relativistic and cold i.e. $\eta = 1$ where the thermal energy of the matter is much lower than the rest-mass energy, the specific energy become unity, i.e. $\dot{E} \sim \dot{M}$.

3.2 Radial Momentum Conservation

The equation for the radial momentum conservation is obtained by the projection of the equation for the energy momentum conservation, $T^{\mu\nu}_{\ ;\nu}=0$, into r-direction, i.e., $h^r_\mu T^{\mu\nu}_{\ ;\nu}=0$. We can write down $h^r_\mu T^{\mu\nu}_{\ ;\nu}=0$ as,

$$a^r=-\frac{h^{rr}}{\rho_0\eta}\frac{dp}{dr}+n_{\rm HI}, \tag{24}$$

where a^r is the radial component of the four-acceleration of the fluid, $a^\mu=u^\mu_{\ ;\nu}u^\nu$, and $n_{\rm HI}$ includes the effects of the heat inertia which are discussed by Beloborodov, Abramowicz & Novikov (1997).

The radial component of the four-acceleration, $a^r(=u^r_{\ ;\nu}u^\nu)$, is calculated as

$$a^r=u^r\frac{du^r}{dr}-n_{\rm acc}, \tag{25}$$

where we decompose $n_{\rm acc}$ into three parts as

$$n_{\rm acc}=n_{\rm KP}(\Omega-\Omega^+_K)(\Omega-\Omega^-_K)+n_{\rm BL}+n_{\rm KS}. \tag{26}$$

Here, $\Omega\equiv u^\phi/u^t$ is the angular velocity and $\Omega^\pm_K$ are the Keplerian angular momentum described as $\Omega^\pm_K=\pm m^{1/2}/(r^{3/2}\pm am^{1/2})$ which are the solutions of $g_{\phi\phi,r}\Omega^2+2g_{t\phi,r}\Omega+g_{tt,r}=0$. The term including $n_{\rm KP}$ measures the deviation of the angular velocity from the Keplerian angular velocity. The terms $n_{\rm KP}$, $n_{\rm BL}$ and $n_{\rm KS}$ are given as

$$n_{\rm KP} \equiv \frac{1}{2}g^{rr}g_{\phi\phi,r}(u^t)^2, \tag{27}$$

$$n_{\rm BL} \equiv -\frac{1}{2}g^{rr}g_{rr,r}(u^r)^2, \tag{28}$$

$$n_{\rm KS} \equiv -(g^{tr}g_{tr,r}+g^{r\phi}g_{r\phi,r})(u^r)^2-\left[g^{tr}\left(g_{tt,r}+g_{t\phi,r}\Omega\right)+g^{r\phi}\left(g_{t\phi,r}+g_{\phi\phi,r}\Omega\right)\right]u^tu^r. \tag{29}$$

Since $n_{\rm KS}$ contains g^{tr} and $g^{r\phi}$ which are null for the Kerr metric written by the Boyer-Lindquist coordinate, this term is newly calculated term in this study which use the Kerr-Schild coordinate. On the other hand, the general form of $n_{\rm HI}$ is described as

$$n_{\rm HI} \equiv -\frac{1}{\rho_0\eta}\left[h^r_\mu t^{\mu\nu}_{\ ;\nu}+h^r_\mu(q^\mu u^\nu+q^\nu u^\mu)_{;\nu}\right] \tag{30}$$

$$= -\frac{1}{\rho_0\eta}\left[\left(\Phi-\frac{1}{3}\Theta t^\gamma_{\ \gamma}+u_\mu u^\nu q^\mu_{\ ;\nu}\right)u^r+t^{r\nu}_{\ ;\nu}+q^r_{;\gamma}u^\gamma+q^r\Theta+u^r_{;\nu}q^\nu\right], \tag{31}$$

where $\Phi\equiv-\sigma_{\mu\nu}t^{\mu\nu}$ is the dissipation function which is calculated in Sec. 3.6 based on the shear stress measured in the FRF, and $-(1/3)\Theta t^\gamma_{\ \gamma}$ represents the compressive heating rate.

If the effects of the dissipation function, Φ, is dominated, $n_{\rm HI}$ is reduced to

$$n_{\rm HI}=-\frac{u^r}{\rho_0\eta}\Phi, \tag{32}$$

and we use this expression in this study.

Finally, from the equation for the radial momentum conservation, we can derive the equation for du^r/dr as,

$$u^r\frac{du^r}{dr}=-\frac{h^{rr}}{\rho_0\eta}\frac{dp}{dr}+n_{\rm acc}+n_{\rm HI}. \tag{33}$$

This equation is used to derive equations which determine the boundary conditions for the sonic point and the viscous point in Sec. 4. In this study, we solve the radial component of the four velocity u^r in the KSR instead of the radial velocity $\hat{v}_r$ measured in the LNRF when we solve the transonic solutions. This is because while $\hat{v}_r$ have the negative and positive values as denoted above, u^r is always negative for the accretion flow. Thus, we choose u^r as one of the basic dynamic variables when solving the transonic flows.

3.3 Angular Momentum Conservation

The equation for the angular momentum conservation is obtained by the projection of the equation for the energy momentum conservation, $T^{\mu\nu}_{\ ;\nu}=0$, into ϕ-direction, i.e., $h^\phi_\mu T^{\mu\nu}_{\ ;\nu}=0$. By using the vertical averaging procedure, we can write down $h^\phi_\mu T^{\mu\nu}_{\ ;\nu}=0$ as,

$$\left[\eta\ell-\frac{4\pi H_\theta\sqrt{-g}}{\dot{M}}(t^r_{\ \phi}+u^rq_\phi-q^r\ell)\right]_{,r}=\frac{4\pi H_\theta\sqrt{-g}}{\dot{M}}\ell q^\theta. \tag{34}$$

From Eq. (34), we obtain

$$\eta\ell - j - \frac{4\pi H_\theta\sqrt{-g}}{\dot{M}} t^r{}_\phi = Q_\ell, \tag{35}$$

where j is the specific angular momentum and Q_ℓ represents the effects of the heat flux defined as

$$Q_\ell \equiv \int_{r_{\rm min}}^{r_{\rm max}} \frac{4\pi H_\theta\sqrt{-g}}{\dot{M}} \ell q^\theta dr + \frac{4\pi H_\theta\sqrt{-g}}{\dot{M}} \left(u^r q_\phi - q^r \ell\right). \tag{36}$$

When the angular momentum is not transported by the heat flux,

$$\dot{M} j = \dot{M}\eta\ell - 4\pi r^2 H_\theta t^r{}_\phi, \tag{37}$$

where the first term in the left-side hand is the total flux of the angular momentum of the fluid, the second term represents the amount of the dissipation due to the shear stress, and the right-hand side is the total inward flux of the angular momentum. In this study, we assume no angular momentum is transported by the heat flux, and in this case the shear stress tensor $t^r{}_\phi$ is written as

$$t^r_\phi = -\rho_0 u^r(\eta\ell - j). \tag{38}$$

3.4 Vertical Structure

The equation for the vertical structure is calculated from the equation of the momentum conservation in θ-direction by assuming the hydrostatic equilibrium. The equation for the momentum conservation in θ-direction is obtained by the projection of the equation for the energy momentum conservation, $T^{\mu\nu}_{\ ;\nu} = 0$, into θ-direction, i.e., $h^\theta_\mu T^{\mu\nu}_{\ ;\nu} = 0$. Although the calculation procedures for the characteristic angular scale of the accretion flow, H_θ, is basically same as those used in Abramowicz, Lanza & Percival (1997), we use several different assumptions. From $h^\theta_\mu T^{\mu\nu}_{\ ;\nu} = 0$, by neglecting the effects due to the heat flux, i.e. $q^\mu = 0$, we obtain

$$\frac{1}{\rho_0\eta}\frac{\partial p}{\partial\theta} = -\left(u^r\frac{\partial u_\theta}{\partial r} + u^\theta\frac{\partial u_\theta}{\partial\theta}\right) + \Gamma^\mu_{\theta\nu}u_\mu u^\nu - \frac{u_\theta}{\eta}\left(u^r\frac{\partial\eta}{\partial r} + u^\theta\frac{\partial\eta}{\partial\theta}\right) - \frac{t^\nu_{\theta;\nu}}{\rho_0\eta} - \frac{(q^\nu u_\theta + q_\theta u^\nu)_{;\nu}}{\rho_0\eta}. \tag{39}$$

Here, the terms including the differentiation of η and $t^\nu_{\theta;\nu}$ are newly considered terms which are not taking into account in Abramowicz, Lanza & Percival (1997) which assume $\eta = 1$. It is note that Popham & Gammie (1998) which do not assume $\eta = 1$ use the equation for H_θ derived by Abramowicz, Lanza & Percival (1997) assuming $\eta = 1$.

We expand the pressure in θ-direction until the order of $\cos^2\theta$ as,

$$p(r,\theta) = p_0(r)\left[1 - \frac{1}{2}\left(\frac{\cos\theta}{H_\theta}\right)^2\right], \tag{40}$$

where $p_0(r)$ is the pressure in the equatorial plane. This expansion is different from the expansion in Abramowicz, Lanza & Percival (1997) by the factor 1/2 before $(\cos\theta/H_\theta)^2$. From this, we can calculate $\partial p/\partial\theta = (2\cos\theta/H_\theta^2)p_0(r)$. From this, the angular half-thickness of the disk is calculated as

$$H_\theta^2 = \left(\frac{p_0}{\rho_0\eta}\right)\Bigg/\left[-u^\nu u_{\theta,\nu} + \Gamma^\mu_{\theta\nu}u_\mu u^\nu - \frac{u_\theta u^\nu\eta_{,\nu}}{\eta} - \frac{t^\nu_{\theta;\nu}}{\rho_0\eta} - \frac{(q^\nu u_\theta + q_\theta u^\nu)_{;\nu}}{\rho_0\eta}\right] \tag{41}$$

In order to expand the denominator of Eq. (50) until the order of $\cos\theta$, we also approximate u_θ as

$$u_\theta(r,\theta) = u_{\theta 1}(r)\cos\theta, \tag{42}$$

where $u_{\theta 1}$ is θ-component of u_μ in the equatorial plane. By using these expansion until the order of $\cos\theta$, we obtain

$$\begin{aligned} -u^\nu u_{\theta,\nu} &= -\left(u^r\frac{\partial u_\theta}{\partial r} + u^\theta\frac{\partial u_\theta}{\partial\theta}\right) \\ &= \cos\theta\left(-u^r u_{\theta 1,r} + g^{\theta\theta}u_{\theta 1}^2\right), \end{aligned} \tag{43}$$

$$\begin{aligned} -\frac{u_\theta u^\nu\eta_{,\nu}}{\eta} &= -\frac{u_\theta}{\eta}\left(u^r\frac{\partial\eta}{\partial r} + u^\theta\frac{\partial\eta}{\partial\theta}\right) \\ &= \cos\theta\left(-u_{\theta 1}u^r\frac{\partial\ln\eta}{\partial r}\right). \end{aligned} \tag{44}$$

In the same way, we can also calculate $\Gamma^\mu_{\theta\nu}u_\mu u^\nu$ and $-t^\nu_{\theta;\nu}/(\rho_0\eta)$ until the order of $\cos\theta$ as,

$$\Gamma^\mu_{\theta\nu}u_\mu u^\nu = \cos\theta\ (\Gamma^\mu_{\theta\nu}u_\mu u^\nu)_1, \tag{45}$$

$$t^\nu_{\theta;\nu}/(\rho_0\eta) = \cos\theta\ [t^\nu_{\theta;\nu}/(\rho_0\eta)]_1, \tag{46}$$

$$(q^\nu u_\theta + q_\theta u^\nu)_{;\nu}/(\rho_0\eta) = \cos\theta\ [(q^\nu u_\theta + q_\theta u^\nu)_{;\nu}/(\rho_0\eta)]_1, \tag{47}$$

where the coefficients of terms of the order of $\cos\theta$ are defined as $(\Gamma^\mu_{\theta\nu}u_\mu u^\nu)_1$, $[t^\nu_{\theta;\nu}/(\rho_0\eta)]_1$ and $[(q^\nu u_\theta + q_\theta u^\nu)_{;\nu}/(\rho_0\eta)]_1$. Direct calculations leads the explicit forms of $(\Gamma^\mu_{\theta\nu}u_\mu u^\nu)_1$ as

$$(\Gamma^{\mu}_{\theta\nu}u_{\mu}u^{\nu})_1 = \ell_*^2/r^2, \tag{48}$$

where ℓ_*^2 is calculated as

$$\ell_*^2 \equiv \ell^2 - a^2(\mathcal{E}^2 - 1). \tag{49}$$

From Eq. (49), $\ell_* = \ell$ when $a = 0$ or $\mathcal{E} = 1$. The form of Eq. (49) is same as the results of Abramowicz, Lanza & Percival (1997) where the Boyer-Lindquist coordinate is used. This is because the transformations for ℓ and $\mathcal{E}$ between the Boyer-Lindquist coordinate and the Kerr-Schild coordinate are given as $\ell_{\rm BL} = \ell_{\rm KS}$ and $\mathcal{E}_{\rm BL} = \mathcal{E}_{\rm KS}$. In Appendix F, we also show the direct derivations of Eq. (49) which is essentially same as the calculations using the Boyer-Lindquist coordinate as shown in Abramowicz, Lanza & Percival (1997), but several points are different. Then, the most general form for H_θ^2 is calculated as

$$H_\theta^2 = \left(\frac{p_0}{\rho_0\eta}\right) \Bigg/ \left\{ \frac{\ell_*^2}{r^2} - u^r u_{\theta,r} + u_\theta \left(u^\theta - u^r \frac{\partial \ln \eta}{\partial r}\right) - \left[\frac{t^{\nu}_{\theta;\nu}}{\rho_0\eta}\right]_1 - \left[\frac{(q^\nu u_\theta + q_\theta u^\nu)_{;\nu}}{\rho_0\eta}\right]_1 \right\}, \tag{50}$$

where all physical values such as c_s, u^r, u^θ etc. are evaluated at the equatorial plane. In the present study, we assume $u_\theta = u_{\theta,r} = 0$ and the negligible effects for the viscosity and the heat flux. These assumptions are basically same as Abramowicz et al. (1997) and Gammie & Popham (1998). For the calculations of the transonic solutions in the later sections, we use the angular half-thickness of the disk described as,

$$H_\theta = \frac{c_s}{\ell_*/r}. \tag{51}$$

3.5 Energy Equation

The equation for the local energy conservation is obtained from $u_\mu T^{\mu\nu}_{\ ;\nu} = 0$ as

$$u^r \left(\frac{du}{dr} - \frac{u+p}{\rho_0}\frac{d\rho_0}{dr}\right) = q^+_{\rm vis} - q^-_{\rm rad}, \tag{52}$$

where

$$q^+_{\rm vis} = \Phi - \frac{1}{3}\Theta t^{\gamma}_{\ \gamma}, \tag{53}$$

$$q^-_{\rm rad} = -q^{\mu}_{\ ;\mu} - q^\mu a_\mu. \tag{54}$$

Here the dissipation function Φ is given in Sec. 3.6 and the second term in the right hand side of $q_{\rm vis}$ side represents the compressive heating rate. On the other hand, in the right hand side of $q^-_{\rm rad}$, $-q^{\mu}_{\ ;\mu}$ is the mass-energy flux transported out (in) to (from) the outside region, and $-q^\mu a_\mu$ is the special relativistic correction to $-q^{\mu}_{\ ;\mu}$ due to the heat inertia of the flux and represents the effects of the redshift of the flux. Since the left-hand-side of Eq. (52) include the change of the entropy, s, as

$$\rho_0 T u^r \frac{ds}{dr} = q^+_{\rm vis} - q^-_{\rm rad}, \tag{55}$$

where $\rho_0 T ds/dr$ represents the advected energy of the accretion flow, this equation represents the energy balance of the accretion flows, i.e. (advection cooling)=(viscous heating)-(radiative cooling). For the isothermal flows or the polytropic flows calculated in the later sections, we do not use the energy equation given by Eq. (52) when we solve the transonic solutions for these flows. On the other hand, for the general equation of state where the pressure and the internal energy usually are the functions of both the rest-mass density ρ_0 and the temperature T, the energy equation given by Eq. (52) is required in order to solve the transonic solution. As an example of such cases, we solve the transonic solutions for the advection dominated accretion flows with the general relativistic equation of state.

3.6 Treatment of Viscosity limited by Causality

The viscosity due to the turbulent motion of magnetic field, fluids and particles such as photons and neutrinos is usually considered in the accretion disk. The effect of viscosity is transported to the finite length with the finite viscous timescale, τ_v, and this transportation is limited by the causality. When the fluid's velocity approach the speed of light as near the horizon, it is expected that the viscous transportation become less effective. In this study, we phenomenologically take into account the causal viscous effects. The valid treatment of the causal viscosity will be required in future studies.

3.6.1 Type A Causal Viscosity : Simple treatment of kinematic viscosity

Here, we consider the kinematic viscosity by taking into account the causality. We use the kinematic viscosity coefficient, ν, in order that the kinematic viscosity vanish on and inside the horizon which is expressed as

$$\nu = \begin{cases} \nu_0 f_c, & \text{for} \quad r_+ < r, \\ 0 & \text{for} \quad r \leqq r_+, \end{cases} \tag{56}$$

where r_+ is the radius of the horizon and ν_0 is the kinematic viscosity coefficient when the effects of the causality is not considered, and f_c is a cut-off function described as (Narayan 1992; Peitz & Appl 1997),

$$f_c = \begin{cases} [1-(\hat{v}/c_v)^2]^2, & \text{for} \quad |\hat{v}| \leqq c_v, \\ 0, & \text{for} \quad |\hat{v}| > c_v. \end{cases} \tag{57}$$

Here, $\hat{v} = (1-\hat{\gamma}^{-2})^{1/2}$ where $\hat{\gamma} = \alpha u^t$. These treatments of the kinematic viscosity is similar to those of Peitz & Appl (1997), but several points and explicit expression are different. By using the kinematic viscosity coefficient defined above, we calculate the shear viscosity tensor $t_{\mu\nu}$ as Navier-Stokes viscosity described as $t_{\mu\nu} = -2\rho_0\eta\nu\sigma_{\mu\nu}$.

3.6.2 Type B Causal Viscosity : Shear stress measured in fluid's rest frame

In relativity, the physical meanings are not usually expressed directly in arbitrary frames. The FRF is the most natural place to evaluate the physical processes. We calculate the shear stress in the FRF as Gammie & Popham (1998) by using the relativistic version for the causal stress prescription proposed by Papaloizou & Szuszkiewicz (1994). We assume the shear stress $t_{(r)(\phi)} = t_{(\phi)(r)} (\equiv S)$ in the FRF. The other components of the shear stress in the FRF except $t_{(r)(\phi)}$ and $t_{(\phi)(r)}$ are assumed to be null. This treatment is same as Gammie & Popham (1998). By using the tetrads connecting the KSF and the FRF, the shear stress $t^r{}_\phi$ is calculated as,

$$t^r{}_\phi = 2\left[e^{r(r)}e_\phi^{\ (\phi)} + e^{r(\phi)}e_\phi^{\ (r)}\right] t_{(r)(\phi)} = FS, \tag{58}$$

where $F \equiv e^{r(r)}e_\phi^{\ (\phi)} + e^{r(\phi)}e_\phi^{\ (r)}$ and tetrads in F are calculated by using the LNRF as $e^{\alpha(\beta)} = e^\alpha{}_{(\beta)} = e^\alpha{}_{\hat{\mu}}e^{\hat{\mu}}{}_{(\beta)}$ ($\alpha = r,\ \beta = r,\ \phi$)and $e_\alpha^{\ (\beta)} = e_\alpha^{\ \hat{\mu}}e_{\hat{\mu}}^{\ (\beta)}$ ($\alpha = \phi,\ \beta = r,\ \phi$). The explicit forms of tetrad components are given in Appendix C. For the finite value of $t_{(r)(\phi)}$, the shear stress measured in the KSF, $t^r{}_\phi$, is not null. This feature is contrasted to the shear stress calculated by using the Boyer-Lindquist coordinate as Gammie & Popham (1998), see Eq. (60) in Gammie & Popham (1998). The equation for the shear stress S is described as (Gammie & Popham 1998)

$$u^r\frac{dS}{dr} = -\frac{S-S_0}{\tau_v}, \tag{59}$$

where τ_v is the relaxation timescale of the viscous diffusion and S_0 is the equilibrium value of the shear stress. The relaxation timescale τ_v is related to the propagation speed of the viscous effects c_v as $c_v = (\nu/\tau_v)^{1/2}$ where ν is the kinematic viscosity. The coefficient of the dynamic viscosity λ is described by the kinematic viscosity ν as $\lambda = \rho_0\eta\nu$. In this study, the relaxation timescale τ_v is assumed as $\tau_v = 1/\Omega$. From these relations, the propagation speed of the viscous effects, c_v, are described by the sound speed, c_s, as $c_v = \alpha^{1/2}c_s$. These treatments are basically same as Gammie & Popham (1998).

From the angular momentum equation (38), the shear stress S is calculated as $S = -\rho_0 u^r(\eta\ell - j - Q_\ell)/F$. By differentiating this equation by r, we obtain dS/dr and substitute dS/dr to Eq. (59). Then, the shear stress S is calculated as,

$$S = \frac{S_0 + \dfrac{\rho_0\eta\tau_v(u^r)^2}{F}\left(\dfrac{d\ell}{dr} + \ell\dfrac{d\ln\eta}{dr} - \dfrac{1}{\eta}\dfrac{dQ_\ell}{dr}\right)}{1 - u^r\tau_v\left(\dfrac{2}{r} + \dfrac{d\ln F}{dr} + \dfrac{d\ln H_\theta}{dr}\right)}. \tag{60}$$

where dQ_ℓ/dr is determined by the heat flux and defined as

$$\frac{dQ_\ell}{dr} = \frac{4\pi H_\theta\sqrt{-g}}{\dot{M}}\ell q^\theta + \left[\frac{4\pi H_\theta\sqrt{-g}}{\dot{M}}\left(u^r q_\phi - q^r\ell\right)\right]_{,r}. \tag{61}$$

From Eq. (34), dQ_ℓ/dr is also calculated as

$$\frac{dQ_\ell}{dr} = \left[\eta\ell - \frac{4\pi H_\theta\sqrt{-g}}{\dot{M}}t^r{}_\phi\right]_{,r}. \tag{62}$$

The equilibrium value of the shear stress S_0 is assumed to be the Navier-Stokes value as

$$S_0 = -2\rho_0\eta\nu\sigma_{(r)(\phi)}. \tag{63}$$

The shear rate $\sigma_{(r)(\phi)}$ in the FRF is calculated by using the shear tensor $\sigma_{\mu\nu}$ in KSF as $\sigma_{(r)(\phi)} = \sigma_{\mu\nu}\ e^\mu{}_{(r)}e^\nu{}_{(\phi)}$. In Appendix E, we give the explicit forms for the shear tensors $\sigma_{\mu\nu}$ and the final form of $\sigma_{(r)(\phi)}$. These calculations are more lengthy than the same calculations using the Boyer-Lindquist coordinate but straightforward. Here, we simply express the shear rate $\sigma_{(r)(\phi)}$ as

$$\sigma_{(r)(\phi)} \equiv \sigma = \sigma_r + \sigma_u \frac{du^r}{dr} + \sigma_\ell \frac{d\ell}{dr}. \tag{64}$$

From Eqs. (60), (63) and (64), we can derive the equation for $d\ell/dr$ having the singular point which we call viscous point.

Based on the shear stress and the shear rate calculated in the last section, the dissipation function Φ is calculated as $\Phi \equiv -\sigma_{\mu\nu} t^{\mu\nu} = -\sigma_{(\alpha)(\beta)} t^{(\alpha)(\beta)} = -2\sigma_{(r)(\phi)} t^{(r)(\phi)}$, and finally we obtain

$$\Phi = -2\sigma S, \tag{65}$$

where σ and S are given by Eqs. (60) and (64).

4 BOUNDARY CONDITIONS

The accretion flows plunging into the black hole supersonically must pass the sonic point where the accretion velocity become larger than the sound speed. On the other hand, when the causal viscosity prescription is used, the accretion flows pass the viscous point where the accretion velocity become larger than the speed of the viscous diffusion. In order to smoothly pass the sonic point and the viscous point, the flows must satisfy the boundary conditions at the sonic point (§4.1) and the viscous point (§4.2). By using the causal viscous prescription, the boundary conditions at the outer regions or the inner regions of the accretion flows are not required. The boundary conditions at the event horizon which are used in some past studies are not required in the present study.

4.1 Boundary Conditions at the Sonic Point

In order to obtain the boundary conditions at the sonic point, we need the equation which do not contain the derivatives except du^r/dr.

The pressure p and the internal energy u of the accreting fluid is usually a function of the rest-mass density ρ_0 and/or the temperature T, i.e. $p = p(\rho_0, T)$ and $u = u(\rho_0, T)$. Then, the derivative dp/dr is calculated as

$$\frac{dp}{dr} = \left(\frac{\partial p}{\partial \rho_0}\right)_T \frac{d\rho_0}{dr} + \left(\frac{\partial p}{\partial T}\right)_{\rho_0} \frac{dT}{dr}, \tag{66}$$

$$\frac{du}{dr} = \left(\frac{\partial u}{\partial \rho_0}\right)_T \frac{d\rho_0}{dr} + \left(\frac{\partial u}{\partial T}\right)_{\rho_0} \frac{dT}{dr}. \tag{67}$$

In the case of the pressure and the internal energy is a function of the rest-mass density only, all the thermodynamic quantities can be written by the rest-mass density only, i.e. $(\partial p/\partial T)_{\rho_0} = (\partial u/\partial T)_{\rho_0} = 0$. In such case, with Eqs. (66), (67) and the mass conservation given by Eq. (18), we can obtain the derivative dp/dr described by the derivatives du^r/dr and $d\ell/dr$ as

$$-\frac{d\ln p}{dr} = P_r + P_u \frac{du^r}{dr} + P_\ell \frac{d\ell}{dr}. \tag{68}$$

Usually, the derivation for the boundary condition at the sonic point become lengthy and complex for the general relativistic accretion flows. Eq. (68) is the key equation in order to simply treat the boundary condition at the sonic point. In the case of the general equation of state where the pressure is a function of both the rest-mass density and the temperature, if we use the energy equation given by Eq. (52), we can also have the derivative dp/dr with the form as Eq. (68). The examples of P_r, P_u and P_ℓ for the isothermal disk, the polytropic disk and the ADAF with the general relativistic equation of state are given in Sec. 7. From Eqs. (32), (64) and (65), the term $n_{\rm HI}$ containing the effects of the heat inertia is calculated as

$$n_{\rm HI} = n^r_{\rm HI} + n^u_{\rm HI} \frac{du^r}{dr} + n^\ell_{\rm HI} \frac{d\ell}{dr}, \tag{69}$$

where

$$n^r_{\rm HI} \equiv \frac{u^r S}{\rho_0 \eta} \sigma_r, \quad n^u_{\rm HI} \equiv \frac{u^r S}{\rho_0 \eta} \sigma_u, \quad n^\ell_{\rm HI} \equiv \frac{u^r S}{\rho_0 \eta} \sigma_\ell. \tag{70}$$

Here, S is calculated from Eqs. (38) and (58) as $S = -\rho_0 u^r (\eta\ell - j)/F$. If the heat inertia effects by the flux is required, we change $n^r_{\rm HI}$ and $n^u_{\rm HI}$ according to Eq. (31). On the other hand, $\mathcal{D}_v$, $\mathcal{N}^r_v$ and $\mathcal{N}^u_v$ are defined in the next section in order to have $d\ell/dr$ with the form described as

$$\mathcal{D}_v \frac{d\ell}{dr} = \mathcal{N}^r_v + \mathcal{N}^u_v \frac{du^r}{dr}. \tag{71}$$

By substituting dp/dr and $n_{\rm HI}$ described by Eq. (68) and (69), respectively, into the radial momentum equation given by Eq. (33), the derivative du^r/dr can be calculated as

$$\frac{du^r}{dr} = \frac{\mathcal{N}_s}{\mathcal{D}_s}, \tag{72}$$

where

$$\mathcal{D}_s = u^r - h^{rr}c_s^2\left(P_u + P_\ell\frac{\mathcal{N}_v^u}{\mathcal{D}_v}\right) - \left(n_{\rm HI}^u + n_{\rm HI}^\ell\frac{\mathcal{N}_v^u}{\mathcal{D}_v}\right), \tag{73}$$

$$\mathcal{N}_s = n_{\rm acc} + h^{rr}c_s^2\left(P_r + P_\ell\frac{\mathcal{N}_v^r}{\mathcal{D}_v}\right) + \left(n_{\rm HI}^r + n_{\rm HI}^\ell\frac{\mathcal{N}_v^r}{\mathcal{D}_v}\right). \tag{74}$$

Here, we use Eq. (71) to remove the derivative $d\ell/dr$.

In order to pass the sonic point smoothly where $\mathcal{D}_s = 0$, the condition $\mathcal{N}_s = 0$ must be satisfied at the sonic point. So, the boundary conditions at the sonic point are

$$\mathcal{D}_s = \mathcal{N}_s = 0. \tag{75}$$

4.2 Another Boundary Condition

4.2.1 For Type A Causal Viscosity: Boundary Condition at Horizon

For the type 1 causal viscosity prescription, we put the boundary condition at the horizon in order to vanish the angular momentum transportation at the horizon. At $r = r_+$, from the condition $\nu = 0$, $\eta\ell = j$ is required and is used as the boundary condition. In this case, the parameters given at the sonic point determine the transonic solution. The differential equation for the angular momentum, ℓ, is calculated from the equation for the angular momentum conservation and the Navier-Stokes prescription of the viscosity as $t_{\mu\nu} = -2\rho_0\eta\nu\sigma_{\mu\nu}$ as

$$\frac{d\ell}{dr} = \frac{1}{h^{rr}}\left(2\sigma^r{}_\phi - u^r{}_{;\phi} - g^{tr}u_{\phi;t} - g^{r\phi}u_{\phi;\phi} + n_{\rm acc}\ell + g^{rr}\Gamma^\mu_{\phi r}u_\mu + \frac{2}{3}\Theta_r u^r\ell - \frac{u^r\ell}{3}\frac{du^r}{dr}\right), \tag{76}$$

where

$$u^r{}_{;\phi} = \frac{1}{2}(g^{tr}g_{t\phi,r} + g^{rr}g_{r\phi,r} + g^{r\phi}g_{\phi\phi,r})u^r - \frac{1}{2}g^{rr}(g_{t\phi,r} + g_{\phi\phi,r}\Omega)u^t, \tag{77}$$

$$u_{\phi;t} = \frac{1}{2}g_{t\phi,r}u^r, \tag{78}$$

$$u_{\phi\phi} = \frac{1}{2}g_{\phi\phi,r}u^r, \tag{79}$$

$$\Gamma^\mu_{\phi r}u_\mu = \frac{1}{2}(g_{t\phi,r} + g_{\phi\phi,r}\Omega)u^t, \tag{80}$$

and Θ_r is given in Appendix. Here, the shear rate $\sigma^r{}_\phi$ is calculated as

$$\sigma^r{}_\phi = \frac{u^r(\eta\ell - j)}{2\eta\nu}, \tag{81}$$

when the value of the kinematic viscosity coefficient is not zero, i.e., $\nu \neq 0$. When $\nu = 0$, this shear rate is zero, i.e. $\sigma^r{}_\phi = 0$.

4.2.2 For Type B Causal Viscosity: Boundary Conditions at Viscous Point

The boundary conditions at the viscous point are calculated from the equation for $d\ell/dr$. In the same way as Eq. (68), the derivatives of η, H_θ and F with respect to r are described by the combinations of du^r/dr and $d\ell/dr$ as

$$\frac{d\ln\eta}{dr} = \eta_r + \eta_u\frac{du^r}{dr} + \eta_\ell\frac{d\ell}{dr}, \tag{82}$$

$$\frac{d\ln H_\theta}{dr} = H_r + H_u\frac{du^r}{dr} + H_\ell\frac{d\ell}{dr}, \tag{83}$$

$$\frac{d\ln F}{dr} = F_r + F_u\frac{du^r}{dr} + F_\ell\frac{d\ell}{dr}. \tag{84}$$

By substituting Eqs. (63), (64), (82), (83) and (84) into Eq. (60) and using the relation $S = -\rho_0 u^r(\eta\ell - j - Q_\ell)/F$, the equation for $d\ell/dr$ containing no derivatives except du^r/dr can be calculated as,

$$\frac{d\ell}{dr} = \frac{\mathcal{N}_v}{\mathcal{D}_v}, \tag{85}$$

where $\mathcal{N}_v = \mathcal{N}_v^r + \mathcal{N}_v^u(du^r/dr)$ and

$$\mathcal{D}_v = 1 - \frac{(u^r)^2}{2\sigma_\ell F c_v^2}\left[1 + \ell\eta_\ell - \frac{\tilde{Q}_\ell}{\eta} + \frac{SF}{\rho_0\eta u^r}G_\ell\right], \tag{86}$$

$$\mathcal{N}_v^r = -\frac{\sigma_r}{\sigma_\ell} + \frac{(u^r)^2}{2\sigma_\ell F c_v^2}\left[\ell\eta_r - \frac{\tilde{Q}_r}{\eta} + \frac{SF}{\rho_0\eta u^r}\left(G_r - \frac{1}{u^r\tau_v}\right)\right], \tag{87}$$

$$\mathcal{N}_v^u = -\frac{\sigma_u}{\sigma_\ell} + \frac{(u^r)^2}{2\sigma_\ell F c_v^2}\left[\ell\eta_u - \frac{\tilde{Q}_u}{\eta} + \frac{SF}{\rho_0\eta u^r}G_u\right]. \tag{88}$$

Here, G_r, G_u and G_ℓ are defined as

$$G_r \equiv 2/r + F_r + H_r,\ G_u \equiv F_u + H_u,\ G_\ell \equiv F_\ell + H_\ell, \tag{89}$$

in order to have the relation

$$\frac{2}{r} + \frac{d\ln F}{dr} + \frac{d\ln H_\theta}{dr} = G_r + G_u\frac{du^r}{dr} + G_\ell\frac{d\ell}{dr}, \tag{90}$$

in the denominator of Eq. (60), and $\tilde{Q}_r$, $\tilde{Q}_u$ and $\tilde{Q}_\ell$ are determined in order to have the relation

$$\frac{dQ_\ell}{dr} = \tilde{Q}_r + \tilde{Q}_u\frac{du^r}{dr} + \tilde{Q}_\ell\frac{d\ell}{dr}. \tag{91}$$

In this study, we neglect the angular momentum loss by the radiation, i.e. we set $\tilde{Q}_r = \tilde{Q}_u = \tilde{Q}_\ell = 0$.

In order to pass the viscous point smoothly where $\mathcal{D}_v = 0$, the condition $\mathcal{N}_v = 0$ must be satisfied at the viscous point. So, the boundary conditions at the viscous point are

$$\mathcal{D}_v = \mathcal{N}_v = 0. \tag{92}$$

5 COUPLED DIFFERENTIAL EQUATIONS TO BE SOLVED

For the general equation of state, the transonic solutions are obtained by numerically solving the coupled differential equations for the dynamic variables, e.g. u^r, ℓ, and the thermodynamic variables, e.g. T. In the case of the special thermodynamic relations, such as the isothermal flows and the polytropic flows, the thermodynamic variables can be calculated from the dynamical variables. In these cases, we only solve the coupled differential equation for the dynamic variables. In this study, we treat the radial component of the four velocity, u^r, and the angular momentum, ℓ, as the basic dynamical variables to be solved. That is, for the case of the special thermodynamic relations where the thermodynamic variables are calculated from the dynamic variables, we solve the coupled differential equations for u^r and ℓ described as

$$\frac{du^r}{dr} = \frac{\mathcal{N}_s}{\mathcal{D}_s}, \tag{93}$$

$$\frac{d\ell}{dr} = \frac{\mathcal{N}_v}{\mathcal{D}_v}\ \left(= \frac{\mathcal{N}_v^r}{\mathcal{D}_v} + \frac{du^r}{dr}\frac{\mathcal{N}_v^u}{\mathcal{D}_v}\right). \tag{94}$$

In the following sections where the transonic solutions for the isothermal flows and the polytropic flows are calculated, we solve these two differential equations.

On the other hand, for the general equation of state, the differential equation for the thermodynamic variables is usually solved in addition to Eqs. (93) and (94). The differential equations for the thermodynamic variables are derived by using the energy equation given by Eq. (52). In this study, we treat the temperature T as the basic thermodynamic variable whose differential equation is numerically solved. The other thermodynamic variables, such as the rest-mass density ρ_0, the sound velocity c_s, are calculated from u^r, ℓ and T by using the mass conservation equation given by Eq. (18) and the equation of state. Here, we derive the general form of the differential equation for T by using the energy equation. By differentiating the mass conservation given Eq. (18), the disk thickness $H_\theta = c_s r/\ell_*$ and the sound velocity $c_s = [p/(\eta\rho_0)]^{1/2}$ with respect to r, we obtain

$$\frac{2}{r} + \frac{d\ln\rho_0}{dr} + \frac{d\ln|u^r|}{dr} + \frac{d\ln H_\theta}{dr} = 0, \tag{95}$$

$$\frac{d\ln H_\theta}{dr} = \frac{d\ln c_s}{dr} + \frac{1}{r} - \frac{1}{\ell_*}\frac{d\ell_*}{dr}, \tag{96}$$

$$2\frac{d\ln c_s}{dr} = \frac{d\ln p}{dr} - \frac{d\ln\rho_0}{dr} + \frac{d\ln\eta}{dr}. \tag{97}$$

Here $d\ell_*/dr$ can be written by the linear combination of du^r/dr and $d\ell/dr$ as

$$\frac{d\ell_*}{dr} = \ell_*^r + \ell_*^u\frac{du^r}{dr} + \ell_*^\ell\frac{d\ell}{dr}, \tag{98}$$

where the coefficients ℓ_*^r, ℓ_*^u and ℓ_*^ℓ can be calculated analytically or numerically. We newly define

$$P_\rho \equiv \left(\frac{\partial\ln p}{\partial\ln\rho_0}\right)_T,\ \ P_T \equiv \left(\frac{\partial\ln p}{\partial\ln T}\right)_{\rho_0},\ \ U_\rho \equiv \left(\frac{\partial\ln u}{\partial\ln\rho_0}\right)_T,\ \ U_T \equiv \left(\frac{\partial\ln u}{\partial\ln T}\right)_{\rho_0},\ \ \eta_\rho \equiv \left(\frac{\partial\ln\eta}{\partial\ln\rho_0}\right)_T,\ \ \eta_T \equiv \left(\frac{\partial\ln\eta}{\partial\ln T}\right)_{\rho_0}. \tag{99}$$

Here, η_ρ and η_T are related to P_ρ, P_T, U_ρ and U_T as $\eta_\rho = (uU_\rho + pP_\rho - u - p)/(\eta\rho_0)$ and $\eta_T = (uU_T + pP_T)/(\eta\rho_0)$. From Eqs. (66), (67), (95), (96) and (97), we obtain the differential equation for T and ρ_0 as

$$\frac{d\ln T}{dr} = T_r + T_u\frac{du^r}{dr} + T_\ell\frac{d\ell}{dr}, \tag{100}$$

$$\frac{d\ln \rho_0}{dr} = \rho_r + \rho_u\frac{du^r}{dr} + \rho_\ell\frac{d\ell}{dr}. \tag{101}$$

Here T_k and ρ_k ($k = r$, u and ℓ) are calculated as

$$T_k = \mathcal{C}_1^T\mathcal{X}_k + \mathcal{C}_2^T q_k^\pm/u^r, \tag{102}$$

$$\rho_k = \mathcal{C}_1^\rho\mathcal{X}_k + \mathcal{C}_2^\rho q_k^\pm/u^r, \tag{103}$$

where $\mathcal{X}_k$ ($k = r$, u and ℓ) are given as

$$\mathcal{X}_r = \frac{3}{r} - \frac{\ell_*^r}{\ell_*},\ \mathcal{X}_u = \frac{1}{u^r} - \frac{\ell_*^u}{\ell_*},\ \mathcal{X}_\ell = -\frac{\ell_*^\ell}{\ell_*}, \tag{104}$$

and $\mathcal{X}_T^1$, $\mathcal{X}_T^2$, $\mathcal{X}_\rho^1$ and $\mathcal{X}_\rho^2$ are given as

$$\mathcal{C}_1^T = \frac{2}{\mathcal{X}_D}\left(U_\rho - \frac{u+p}{u}\right),\ \ \mathcal{C}_2^T = \frac{1}{u\mathcal{X}_D}(P_\rho - \eta_\rho + 1),\ \ \mathcal{C}_1^\rho = -\frac{2U_T}{\mathcal{X}_D},\ \ \mathcal{C}_2^\rho = -\frac{(P_T - \eta_T)}{u\mathcal{X}_D}, \tag{105}$$

Here, $\mathcal{X}_D$ is defined as

$$\mathcal{X}_D \equiv (P_\rho - \eta_\rho + 1)U_T - (P_T - \eta_T)\left(U_\rho - \frac{u+p}{u}\right). \tag{106}$$

On the other hand, $q_k^\pm$ ($k = r$, u and ℓ) are defined to satisfy the relation

$$q_{\rm vis}^+ - q_{\rm rad}^- = q_r^\pm + q_u^\pm\frac{du^r}{dr} + q_\ell^\pm\frac{d\ell}{dr}. \tag{107}$$

By using the coefficients T_k and ρ_k ($k = r$, u and ℓ) calculated above, the coefficients P_k, η_k and H_k ($k = r$, u and ℓ) are calculated as

$$P_k = -P_T T_k - P_\rho\rho_k, \tag{108}$$

$$\eta_k = \eta_T T_k + \eta_\rho\rho_k. \tag{109}$$

From Eq. (95), we obtain

$$H_r = -\frac{2}{r} - \frac{\rho_r}{\rho_0},\ H_u = -\frac{1}{u^r} - \frac{\rho_u}{\rho_0},\ H_\ell = -\frac{\rho_\ell}{\rho_0}. \tag{110}$$

For the general equation of state, the transonic solutions are obtained by solving the differential equations of u^r, ℓ and T given by Eqs. (93), (94) and (100). In the later sections, for the ADAF with the general relativistic equation of state and the supercritical accretion disk, we solve the differential equations for u^r, ℓ and T. Since the rest-mass density ρ_0 is calculated from the mass conservation equation given by Eq. (18), we do not solve the differential equation for ρ_0.

6 CALCULATION METHOD

By using the formalism developed until the last sections, we solve the coupled differential equations to obtain the transonic solutions. The calculation method for the transonic solutions are not unique, and actually, past studies use several method. Here, we show one of the calculation methods to obtain the transonic solutions.

(i) First, we tentatively choose some value of T_s (or $a_{s,s}$) for given values of r_s and j, and calculate u_s^r, ℓ_s, $(du^r/dr)_s$, $(d\ell/dr)_s$ and $(dT/dr)_s$. Here, the differential values at the sonic point are calculated by using the L'Hopital's rule.

(ii) Next, we solve the solutions in the range $r_s < r < r_v$. In order to do this, we solve the coupled differential equations for u^r, ℓ and T from the sonic point to the viscous point by using, e.g., the Runge-Kutta algorithm. Usually, for the initially selected value of T_s (or $a_{s,s}$), the calculated solution does not pass the viscous point where two boundary conditions $\mathcal{D}_v = \mathcal{N}_v = 0$ are satisfied. In such case, we return to step 1 and again choose the different values of T_s (or $a_{s,s}$) for given values of r_s and j. After repeating these procedures, we can determine the value T_s (or $a_{s,s}$) which gives the solution satisfying the boundary conditions $\mathcal{D}_s = \mathcal{N}_s = 0$ at $r = r_s$ and $\mathcal{D}_v = \mathcal{N}_v = 0$ at $r = r_v$.

(iii) After solving the solutions in $r_s < r < r_v$, we solve the coupled differential equations in the range $r_v < r$ by using the values of T_s (or $a_{s,s}$) for given values of r_s and j by using, e.g., the Runge-Kutta algorithm.

(iv) Finally, we solve the coupled differential equations in the range $r < r_s$ by using the values of T_s (or $a_{s,s}$) for given values of r_s and j by using, e.g., the Runge-Kutta algorithm. If the solutions are connected with the horizon as usual solutions,

we can solve the solutions inside the horizon. On the other hand, if the solutions are not connected with the horizon as the alpha-type solutions, the numerical integrations are stopped before the horizon because there is no stationary solutions for such parameters of r_s and j.

The third step and the fourth step can be interchanged. By this procedure, the transonic solutions are obtained for given values of r_s and j without the boundary conditions for the inner regions ($r < r_s$) of the outer regions ($r_v < r$). By using these procedures, we can basically cover all the possible values of r_s and j. That is, by these methods, in principle, all the possible stationary transonic solutions can be calculated because we can use all the possible sonic point, and the transonic solution is calculated from the sonic point.

7 APPLICATIONS AND SAMPLE SOLUTIONS

In this section, we give the numerical solutions for the ideal isothermal accretion flow (§7.1), the polytropic disks (§7.2), the ADAF with relativistic equation of state (§7.3) and the adiabatic accretion flow (§7.4) and the formulation for the supercritical accretion flow (§7.5). Based on the thermodynamic relations, we first calculate the coefficients P_k, η_k and H_k ($k = r$, u and ℓ) which are used in the calculations of du^r/dr and $d\ell/dr$. In addition, we calculate T_k ($k = r$, u and ℓ) if required. For the ideal flows, we only solve the differential equation of u^r. For the viscous polytropic flows, we solve the coupled differential equations of u^r and ℓ. For ADAFs with the relativistic equation of state, in addition to the differential equation of u^r and ℓ, we also solve the differential equation of T simultaneously, which is derived by using the energy equation. In this section, for the viscous solutions, the kinematic viscosity ν is assumed to described by the alpha viscosity α_v as $\nu = \alpha_v c_s^2/\Omega$.

7.1 Application 1 : Ideal Isothermal Accretion Flow

By using the formalism developed until the last sections, we first shows the numerical solutions of the horizon-penetrating solutions for the ideal isothermal accretion flow which is one of the simplest transonic accretion flow. Here, we only solve the differential equation for u^r by assuming constant specific angular momentum ℓ and sound speed c_s, and $\eta = 1$ is also assumed. We use the coefficients P_r, P_u and P_ℓ described as

$$P_r = \frac{3}{r}, \quad P_u = \frac{1}{u^r}, \quad P_\ell = 0. \tag{111}$$

By substituting Eqs. (111) into Eqs. (72), the differential equation for u^r for the ideal isothermal flows are obtained. We numerically solve this differential equation for u^r and obtain the transonic solutions. When calculating the numerical solutions, the rest-mass density ρ_0 is determined from u^r, ℓ and c_s by using the mass conservation equation given by Eq. (18). For the ideal isothermal flows which are solved in this section, since we assume constant ℓ, there is no viscous point in the global solution of the transonic accretion flow.

In Fig. 1, in the parameter spaces r_s-c_s^2 we plot lines of constant critical values of $\lambda(\equiv -u_\phi/u_t)$. The critical sound speed c_s^2 is plotted for non-rotating ($a/m = 0$:*left panel*) and rotating (0.95: *right panel*) black holes. We calculate transonic solutions with the critical values plotted by the filled triangles in Fig. 1. The resultant transonic solutions for non-rotating black holes are plotted in Fig. 2. We also give the transonic solutions for rotating black holes in Fig. 3. For both Fig. 2 and Fig. 3, the transonic solutions calculated by using the Kerr-Schild coordinate (*left column*) or the Boyer-Lindquist coordinate (*right column*) are plotted. The angular velocity Ω and u^t directly reflect the effects of the coordinate singularity when we use the Boyer-Lindquist coordinate. That is, for the solutions calculated in the Boyer-Lindquist coordinate, the angular velocity, Ω, is equal to the angular velocity of the frame dragging, ω, at the horizon, and u^t is diverged at the horizon. These features are clearly seen in both Fig. 2 and Fig. 3. We also show $\Omega - \omega$ in the inserted box in the panel showing Ω in the right column of Fig. 3. The feature that the angular velocity of the accretion flow written by the Boyer-Lindquist coordinate is equal to the angular velocity of the black hole $\omega = a/2mr$ at the horizon is pointed out by Komissarov (2004) who also found that u^t remains finite at the event horizon and Ω differs from the angular velocity of the black hole in Kerr-Schild coordinate. The coordinate singularity in Boyer-Lindquist coordinate is also relevant to the feature that the world lines of Boyer-Lindquist LNRF become null on the event horizon and thus cannot correspond to any physical observer. For the outside region of the horizon, the lines for u^r are same for both calculations using Kerr-Schild coordinate and the Boyer-Lindquist coordinate. We plot two types of transonic solutions which have the sonic radius in the inside region or the outside region. These two types of solutions correspond to the solutions named type I and type II in Peitz & Appl (1997). Similar solution patterns are also obtained by Fukue (1987).

For the accretion flows calculated by using the Boyer-Lindquist coordinate, we also plot the results for the flows which are firstly calculated based on the Boyer-Lindquist coordinate and then transformed to the flows written by the Kerr-Schild coordinate by the transformations of four velocity given by Eqs. (10) and (11). These results are plotted by the short dashed lines in the right panels for Ω and u^t of Figs. 2 and Fig. 3. These solutions outside the event horizon are same as those calculated based on the Kerr-Schild coordinate presented in the left panels of Figs. 2 and Fig. 3.

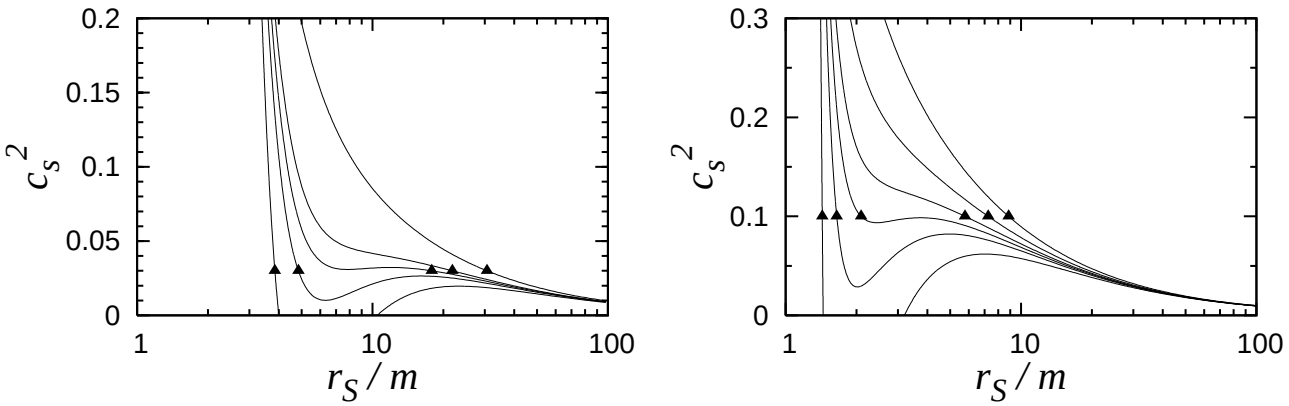

Figure 1. Parameter spaces r_S-c_s^2 showing lines of constant critical values of $\lambda(\equiv -u_\phi/u_t)$. The critical sound speed c_s^2 is plotted for non-rotating ($a/m = 0$:*left panel*) and rotating (0.95: *right panel*) black holes. For non-rotating black holes, contours correspond to $\lambda = 2.0$, 3.2, 3.4, 3.6 and 4.0 (from right to left). For rotating black holes, contours correspond to $\lambda = 1.5$, 1.9, 2.1, 2.2, 2.3 and 2.5 (from right to left). Transonic solutions with the critical values plotted by the filled triangles are calculated in Fig. 2 for non-rotating black holes and in Fig. 3 for rotating black holes.

Outside the horizon, from the results for the accretion flow calculated by using the Boyer-Lindquist coordinate shown in the right panels of Figs. 2 and 3, we can obtain the solutions given in the left panels for the Kerr-Schild coordinate by using the transformation given by Eqs. (10) and (11). While for the ideal accretion flows the accretion flows calculated by these two procedures have same results, for the viscous flows the solutions calculated by these two procedures do not have the exactly same results. See the discussion in the last section.

7.2 Application 2 : Polytropic Accretion Flow

Here, we show the transonic accretion flows with the polytropic equation flows. Although this equation determine the general energy equation, in this paper, we only consider the accretion flows with the polytropic equation of state as

$$p = K\rho_0^\Gamma, \tag{112}$$

where K is constant and Γ is the adiabatic index (or the ratio of specific heat). The adiabatic index Γ is related to the polytropic index N as $\Gamma = 1 + 1/N$. The internal energy u is given by $u = p/(\Gamma - 1)$. When solving the transonic solutions for polytropic accretion flows, we do not use the energy equation in Eq. (52). All the thermodynamic variables are expressed by the rest-mass density ρ_0 for given adiabatic index Γ and the constant K. The relativistic enthalpy η [$= 1 + (u + p)/\rho_0$] and the sound speed c_s [$= p/(\rho_0\eta)$] are calculated as

$$\eta = 1 + \left(\frac{\Gamma}{\Gamma - 1}\right)\frac{p}{\rho_0}, \tag{113}$$

$$c_s^2 = \frac{p}{\rho_0 + [\Gamma/(\Gamma - 1)]p}. \tag{114}$$

From Eqs. (112), (113) and (114), dp/dr, $d\eta/dr$ and dc_s/dr and can be calculated from $d\rho_0/dr$ as

$$\frac{dp}{dr} = \frac{\Gamma p}{\rho_0}\frac{d\rho_0}{dr}, \tag{115}$$

$$\frac{d\eta}{dr} = \frac{\Gamma p}{\rho_0^2}\frac{d\rho_0}{dr}, \tag{116}$$

$$\frac{dc_s}{dr} = \frac{(\Gamma - 1)c_s}{2\eta\rho_0}\frac{d\rho_0}{dr}. \tag{117}$$

From the disk thickness given by Eq. (51) and the mass conservation given by Eq. (18), we obtain Eqs. (95) and (96). By eliminating dH_θ/dr from Eqs. (95) and (96) and substituting Eq. (117), the derivative $d\rho_0/dr$ is calculated as,

$$\frac{d\rho_0}{dr} = \frac{-2\eta\rho_0}{2\eta + \Gamma - 1}\Big[\frac{4}{r} - \frac{\ell_*^r}{\ell_*} + \Big(\frac{1}{u^r} - \frac{\ell_*^u}{\ell_*}\Big)\frac{du^r}{dr} - \frac{\ell_*^\ell}{\ell_*}\frac{d\ell}{dr}\Big]. \tag{118}$$

By substituting Eq. (118) into Eq. (115), P_r, P_u and P_ℓ are calculated as,

$$P_r = \mathcal{X}_p\Big(\frac{4}{r} - \frac{\ell_*^r}{\ell_*}\Big),\ P_u = \mathcal{X}_p\Big(\frac{1}{u^r} - \frac{\ell_*^u}{\ell_*}\Big),\ P_\ell = -\mathcal{X}_p\frac{\ell_*^\ell}{\ell_*}. \tag{119}$$

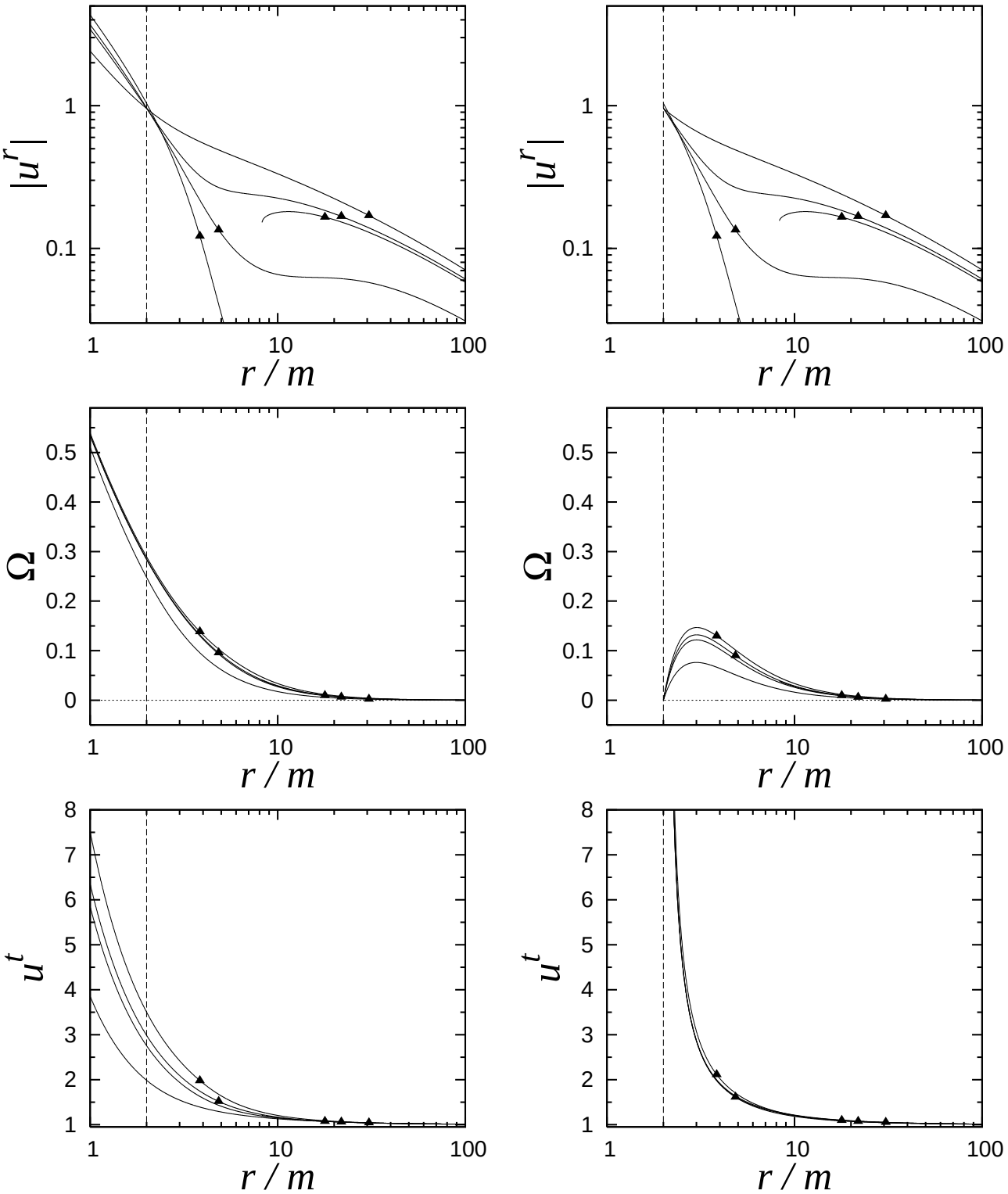

Figure 2. Sample transonic solutions for the ideal isothermal flows when $a/m = 0$. We plot transonic solutions with the critical values $\lambda = 2.0$, 3.2, 3.4, 3.6 and 4.0 (from right to left) with the sound speed $c_s^2 = 0.03$. The transonic solutions calculated by using the Kerr-Schild coordinate (*left column*) or the Boyer-Lindquist coordinate (*right column*) are plotted. The radius of the horizon is denoted by the dashed line, and the angular velocity of the frame dragging is plotted by the dotted lines in the panel showing Ω.

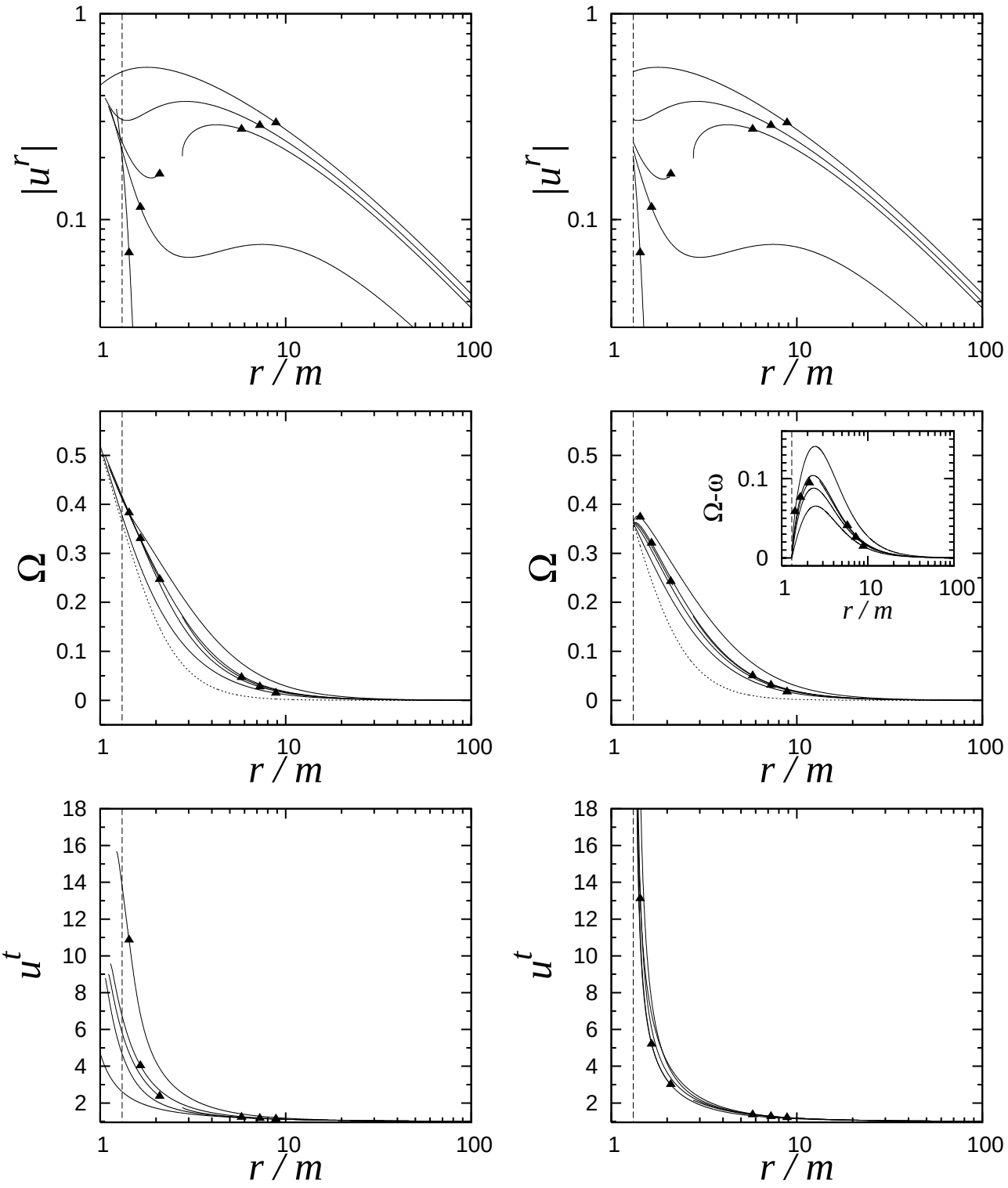

Figure 3. Sample transonic solutions for the isothermal ideal flows when $a/m = 0.95$. We plot transonic solutions with the critical values $\lambda = 1.5$, 1.9, 2.1, 2.2, 2.3 and 2.5 (from right to left) with the sound speed $c_s^2 = 0.1$. The transonic solutions calculated by using the Kerr-Schild coordinate (*left column*) or the Boyer-Lindquist coordinate (*right column*) are plotted. The radius of the horizon is denoted by the dashed line, and the angular velocity of the frame dragging is plotted by the dotted lines in the panel showing Ω. We also show $\Omega - \omega$ in the inserted box in the panel showing Ω in the right column.

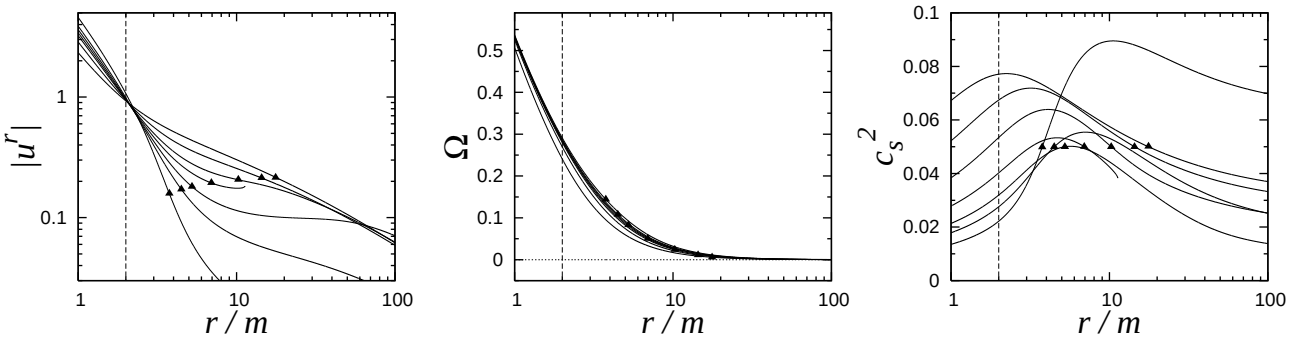

Figure 4. Sample transonic solutions for the polytropic ideal flows for $a/m = 0$. We plot transonic solutions with the critical values $\lambda = 2.0$, 2.6, 3.0, 3.2, 3.4, 3.6 and 4.0 (from right to left) with the critical sound speed $c_s^2 = 0.05$. The radius of the horizon is denoted by the dashed line, and the sonic points are plotted by the filled triangles.

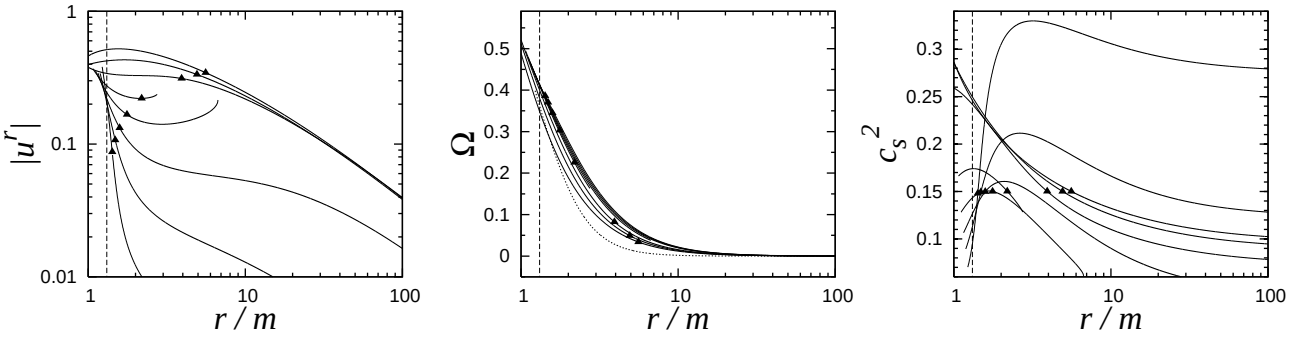

Figure 5. Sample transonic solutions for the polytropic ideal flows for $a/m = 0.95$. We plot transonic solutions with the critical values $\lambda = 1.5$, 1.7, 1.9, 2.1, 2.2, 2.3, 2.4 and 2.5 (from right to left) with the critical sound speed $c_s^2 = 0.15$.

Here, we define $\mathcal{X}_p \equiv 2\eta\Gamma/(2\eta + \Gamma - 1)$. In the same way, η_r, η_u and η_ℓ are calculated as,

$$\eta_r = -c_s^2 P_r, \quad \eta_u = -c_s^2 P_u, \quad \eta_\ell = -c_s^2 P_\ell, \tag{120}$$

and H_r, H_u and H_ℓ are calculated as,

$$H_r = -\mathcal{X}_p\Big(\frac{\Gamma-1}{\eta r} - \frac{1}{r} + \frac{\ell_*^r}{\ell_*}\Big), \quad H_u = -\mathcal{X}_p\Big(\frac{\Gamma-1}{2\eta u^r} + \frac{\ell_*^u}{\ell_*}\Big), \quad H_\ell = -\mathcal{X}_p\Big(\frac{\ell_*^\ell}{\ell_*}\Big). \tag{121}$$

By substituting Eqs. (119), (120) and (121) into Eqs. (72) and (85), the differential equations for u^r and ℓ for the polytropic accretion flows are described as $du^r/dr = \mathcal{N}_s/\mathcal{D}_s$, $d\ell/dr = \mathcal{N}_v^r/\mathcal{D}_v + (\mathcal{N}_v^u/\mathcal{D}_v)du^r/dr$ which are the basic coupled differential equations to be solved. In this section, we calculate the ideal polytropic flows and the viscous polytropic flows. For the ideal polytropic flows, we assume $\eta\ell$ =constant and only solve the differential equation for u^r, and the global transonic solutions do not have the viscous point. For the viscous polytropic flows, we solve the coupled differential equations of u^r and ℓ, and obtain the transonic solutions satisfying the boundary conditions at the sonic point and the viscous point. For all the viscous flows, we assume the alpha viscosity $\alpha_v = 0.1$. The radius of the sonic point is determined in order to pass the viscous point. In the same way as the previous section, when calculating the numerical solutions, the rest-mass density ρ_0 is determined from u^r, ℓ and c_s by using the mass conservation equation given by Eq. (18).

We show the sample solutions for the horizon-penetrating transonic solutions of the ideal polytropic flows for $a/m = 0$ and 0.95 in Fig. 4 and Fig. 5, respectively. The sonic points are plotted by the filled triangles, and the radius of the horizon is plotted by the dashed lines. The transonic solutions for the viscous polytropic flows for $a/m = 0$ and 0.95 are given in Fig. 6 and Fig. 7, respectively. For the viscous flows, the sonic points and the viscous points are plotted by the filled triangles and squares, respectively. All the viscous polytropic solutions presented here become super-Keplerian flows in the outer region, and the sound speed diverged. The outer region of these solutions correspond to the thick disk solutions.

7.3 Application 3 : ADAFs with Relativistic Equation of State

Here, we calculate the transonic solutions for the ADAF with relativistic equation of state. where the energy equation given by Eq. (52) is required in order to close the coupled differential equations. For the Boyer-Lindquist coordinate which have the

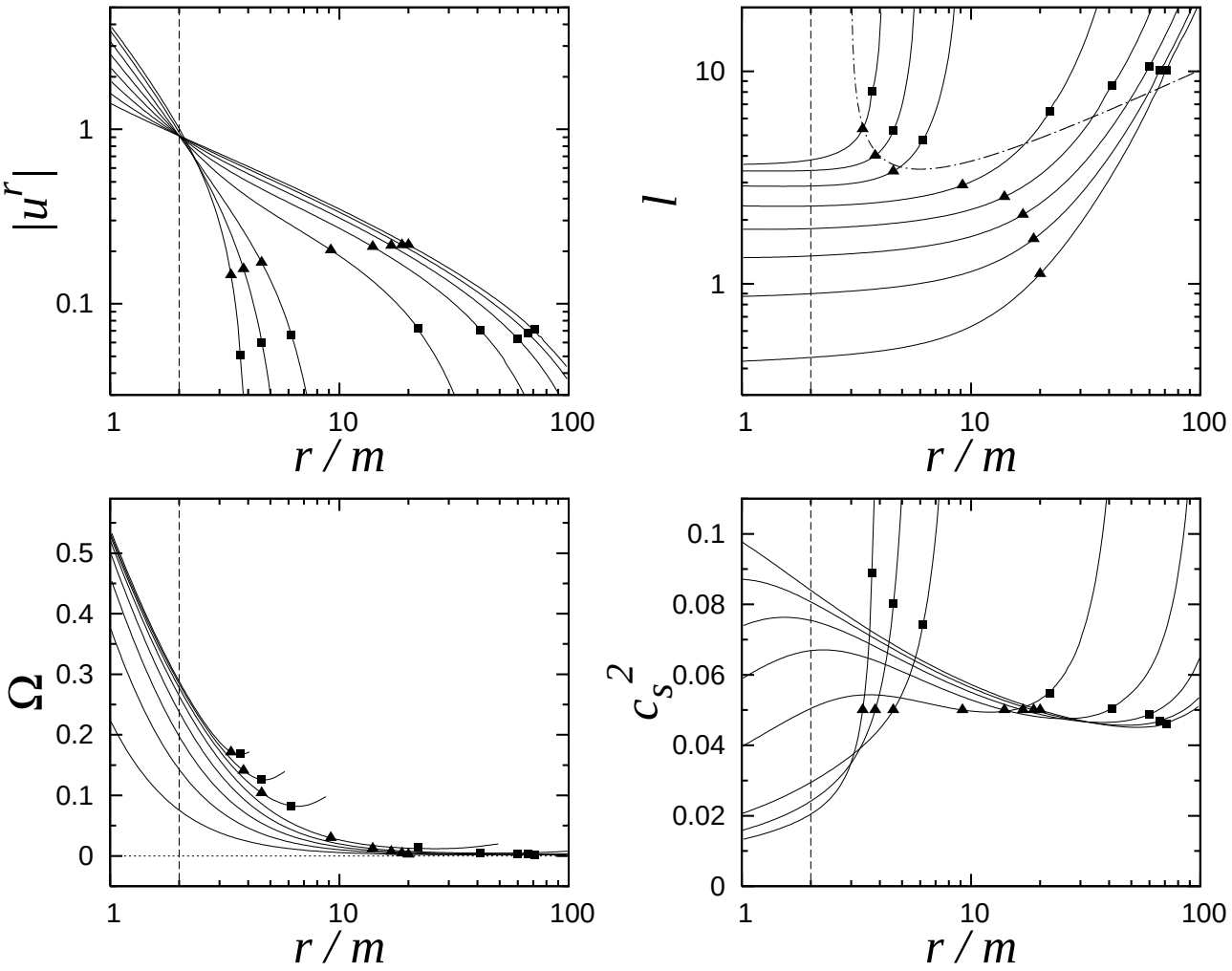

Figure 6. Sample transonic solutions for the viscous polytropic flows when $a/m = 0$. We plot transonic solutions with the constant specific angular momentum $j = 0.5$, 1.0, 1.5, 2.0, 2.5, 3.0, 3.5 and 3.7 (from right to left) with the critical sound speed $c_s^2 = 0.05$. The radius of the horizon is denoted by the dashed line. The sonic points and the viscous points are plotted by the filled triangles and squares, respectively.

coordinate singularity at the horizon, Gammie & Popham (1998) and Popham & Gammie (1998) solve the transonic solutions by using the causal viscosity prescription.

Here, we use the equation of state same as Gammie & Popham (1998). The pressure p and the internal energy u is given by the rest-mass density ρ_0 and the temperature T as (Chandrasekhar 1939; Cox & Giuli 1968)

$$p = \rho_0 T, \tag{122}$$

$$u = \rho_0 \left[3T + \frac{K_1(1/T)}{K_2(1/T)} \right], \tag{123}$$

where K_n's are the modified Bessel functions of the second kind of order n. The internal energy u is well fitted by the function as (Gammie & Popham 1998) $u = \rho_0 T g(T)$ where $g(T) = (45T^2 + 45T + 12)/(15T^2 + 20T + 8)$. The relativistic enthalpy η and the sound velocity c_s become a function of the temperature T as,

$$\eta = 1 + T\left[1 + g(T)\right], \qquad c_s^2 = \frac{T}{1 + T[1 + g(T)]}. \tag{124}$$

Here, η and c_s are functions of temperature, T. By using these equations, we can obtain

$$P_\rho = 1, \quad P_T = 1, \quad U_\rho = 1, \quad U_T = 1 + \frac{d\ln g(T)}{d\ln T}, \quad \eta_\rho = 0, \quad \eta_T = \frac{1}{\rho_0 \eta}\left(1 + u + u\frac{d\ln g(T)}{d\ln T}\right). \tag{125}$$

On the other hand, by using the assumption $q^-_{\rm rad} = 0$, we can calculate the coefficients $q^\pm_k$ ($k = r$, u and ℓ) as

$$q^\pm_k = -2S\sigma_k. \tag{126}$$

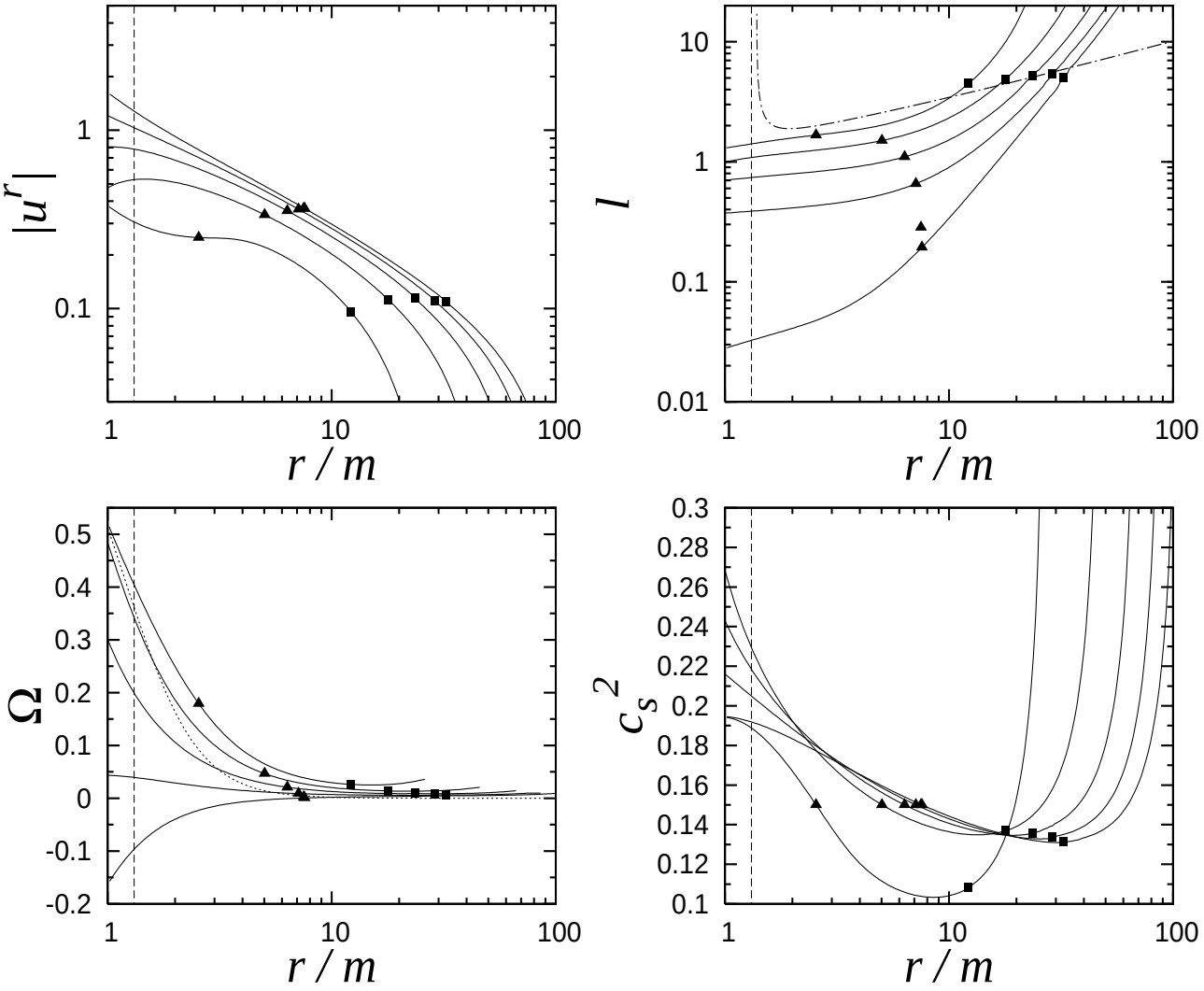

Figure 7. Sample transonic solutions for the viscous polytropic flows when $a/m = 0.95$. We plot transonic solutions with the constant specific angular momentum $j = 0.01$, 0.5, 1.0, 1.5 and 1.8 (from right to left) with the critical sound speed $c_s^2 = 0.15$.

By substituting equations given by Eq. (125) into Eqs. (102), (108) and (110), we can calculate the coefficients P_k, H_k, η_k and T_k ($k = r$, u and ℓ). Now, it is noted that the relativistic enthalpy η is also calculated by the equation in Eq. (124). Then, the derivatives du^r/dr, $d\ell/dr$ and dT/dr are obtained and numerically solved in order to calculate the transonic solutions for the adiabatic accretion disks. In Fig. 8, we show the sample numerical transonic solutions for the ADAF with the relativistic equation of state. Sample numerical solutions are calculated for $a/m = 0.0$, 0.5, 0.95 and 0.99999 with $T_s = 0.1$, and we plot the four-velocity components, u^r and u^t, the angular velocity Ω, the dimensionless temperature T, the relativistic enthalpy η and $\eta\ell$. The solutions are calculated so as to satisfy zero shear stress at the horizon. The positions of the horizons and the sonic points are denoted by the blank circles and the filled triangles, respectively. The dashed lines in the panel for $\eta\ell$ (*bottom right*) are the angular momentum for the Keplerian motion when $a/m = 0.0$, 0.5, 0.95 and 0.99999 (right to left). All solutions pass the event horizon smoothly and have nearly same flow patterns in the outer region. As denoted in the previous section, the accretion flow is plunging into the black hole with the angular velocity which is different from the angular velocity of the black hole's rotation at the event horizon. While the accretion flow have the smaller values of $|u^r|$ for larger values of black hole spins, the gamma factor $\gamma = \alpha u^t$ become larger for the larger values of the black hole spins. This is because of the effects of the black hole rotation enhances the rotational velocity of the accretion flow, i.e., for larger black hole spins the accretion flows have the larger values of the angular three velocity. The relativistic enthalpy $\eta = 1 + (u+p)/\rho_0$ of the hot accretion flow is in general larger than unity near the horizon. In the sample solutions for $a/m = 0.95$ and 0.99999, the accretion flows are sub-Keplerian in all the region. On the other hand, for $a/m = 0.5$, the middle part of the accretion flow is super-Keplerian. The similar feature is also pointed out by Peitz & Appl (1997).

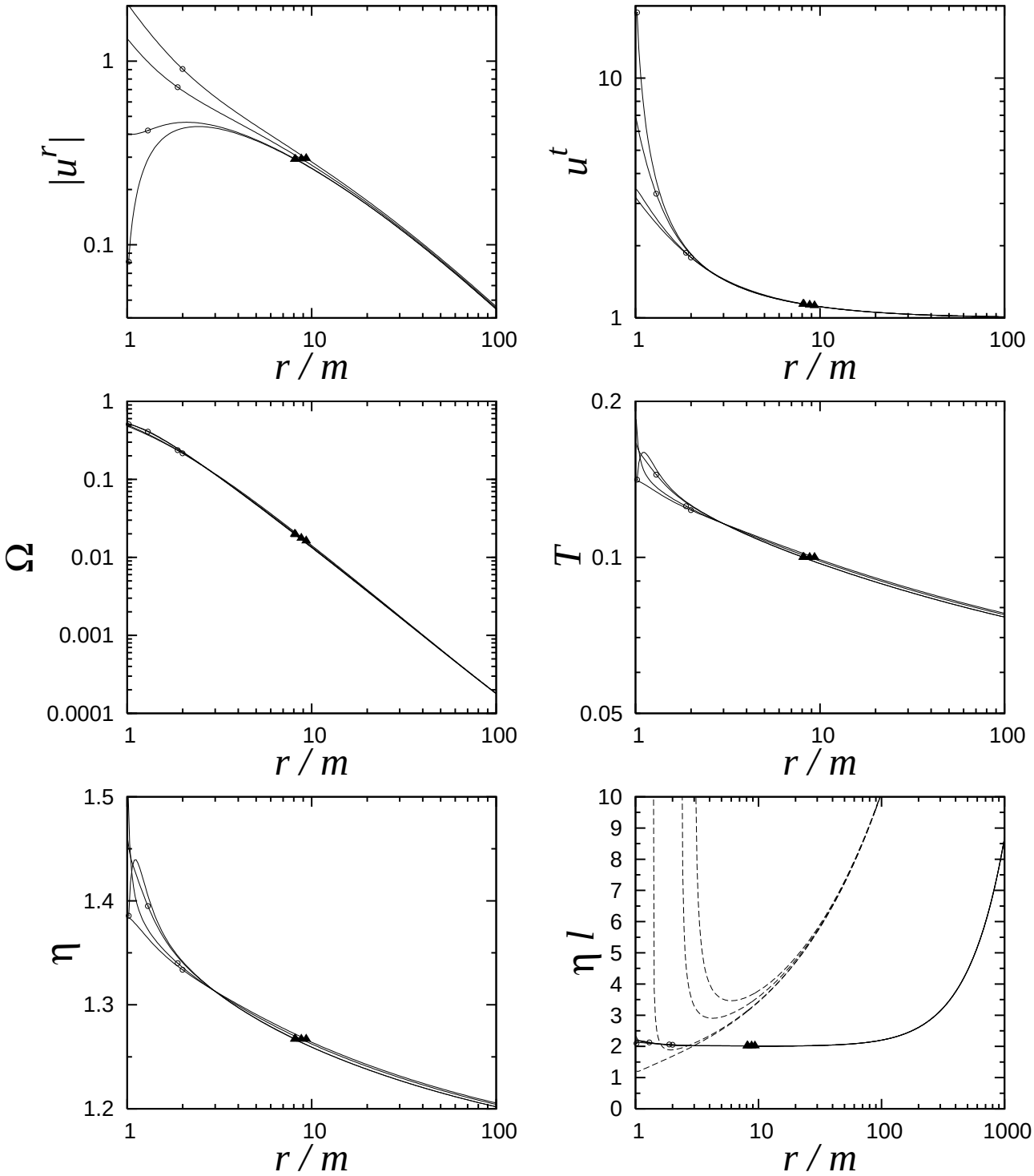

Figure 8. Sample numerical solutions for transonic accretion flows of ADAFs with relativistic equation of state when $a/m = 0.0$, 0.5, 0.95 and 0.99999 with $T_s = 0.1$. We plot the four-velocity components, u^r and u^t, the angular velocity Ω, the dimensionless temperature T, the relativistic enthalpy η and $\eta\ell$. The solutions are calculated so as to satisfy zero shear stress at the horizon. The positions of the horizons and the sonic points are denoted by the blank circles and the filled triangles, respectively. The dashed lines in the panel for $\eta\ell$ (*bottom right*) are the angular momentum for the Keplerian motion when $a/m = 0.0$, 0.5, 0.95 and 0.99999 (right to left). Here, we assume the alpha viscosity parameter 0.01 and type A causal viscosity.

7.4 Application 4 : Adiabatic Accretion Disk and Standard Accretion Disk

In this section, we calculate the accretion flows where the viscous heating rate is balanced with the radiative cooling rate, $q^+_{\rm vis} = q^-_{\rm rad}$. This assumption is usually used in the calculations of the standard accretion disks. From this assumption and the energy equation given by Eq. (55), we can show that the entropy change of the accretion flow is zero, i.e. $dS = 0$. So, here, we call the disk with this assumption as adiabatic accretion disk.

Here, we calculate the transonic solutions for the adiabatic accretion disks whose mass accretion rate is near or beyond the Eddington mass accretion rate. For the supercritical accretion flow the contribution from the radiation pressure of photons can not be neglected. When the specific heat at the constant volume, c_V, is independent of the temperature, the pressure p and the internal energy u for the flows containing gas and radiation are given as (Chandrasekhar 1939),

$$p = p_g + p_r, \tag{127}$$

$$u = \frac{1}{\gamma - 1} p_g + 3p_r, \tag{128}$$

where p_g and p_r are the gas pressure and the radiation pressure, respectively, described as

$$p_g = \frac{k_B}{\mu m_H}\rho_0 T, \qquad p_r = \frac{1}{3} a_{\rm rad} T^4. \tag{129}$$

Here, γ is the ratio of the specific heats, k_B is the Boltzmann constant, μ is the mean molecular weight, m_H is the Hydrogen mass, $a_{\rm rad}$ is the radiation constant, and we use the dimensional representation of the pressures. These assumptions are sometimes used in the past studies for the standard accretion disk (e.g. Shakura & Sunyaev 1973, Novikov & Thorne 1974, Page & Thorne 1974, Matsumoto et al. 1984). For flows with $dS = 0$, the energy equation, $u^r \rho_0 T(dS/dr) = q^+_{\rm vis} - q^-_{\rm rad}(= 0)$, can be given by using the generalized adiabatic exponents as

$$\frac{u^r}{\Gamma_3 - 1}\left(\frac{dp}{dr} - \Gamma_1 \frac{p}{\rho_0}\frac{d\rho_0}{dr}\right) = q^+_{\rm vis} - q^-_{\rm rad}(= 0), \tag{130}$$

where

$$\Gamma_1 = \beta + \frac{(4-3\beta)^2(\gamma-1)}{\beta + 12(\gamma-1)(1-\beta)}, \tag{131}$$

$$\Gamma_3 = 1 + \frac{\Gamma_1 - \beta}{4 - 3\beta}. \tag{132}$$

Here, β is the ratio of the gas pressure to the total pressure, i.e. $\beta \equiv p_g/p$. In the calculations of the transonic flows, we use the dimensionless pressure, internal energy, rest-mass density and the temperature. By using the dimensionless prescription, the pressure and the internal energy can be calculated as $p = p_g + p_r$ and $u = p_g/(\gamma - 1) + 3p_r$ where $p_g = \rho_0 T$ and $p_r = T^4/3$ where the temperature is normalized by $m_p c^2/k_B$, the rest-mass density is firstly normalized by $(a_{\rm rad}/c^2)(m_p c^2/k_B)^4$ to the dimensionless quantities and is secondly normalized so as to satisfy $\dot{M} = 1$. Here, m_p is the proton mass and c is the speed of light. Since the left-hand-side of Eq. (130) derived from the condition $dS = 0$ is equivalent to that of Eq. (55), we have the relations

$$\left(\frac{\partial u}{\partial T}\right)_{\rho_0} = \frac{1}{\Gamma_3 - 1}\left(\frac{\partial p}{\partial T}\right)_{\rho_0}, \tag{133}$$

$$\left(\frac{\partial u}{\partial \rho_0}\right)_{T} = \frac{1}{\Gamma_3 - 1}\left[\left(\frac{\partial p}{\partial \rho_0}\right)_{T} - \Gamma_1 \frac{p}{\rho_0}\right] + \frac{u+p}{\rho_0}. \tag{134}$$

From the equation of state and Eqs. (133) and (134), we have

$$P_\rho = \beta, \quad P_T = 4 - 3\beta, \quad U_\rho = -\frac{p}{u}\left[2(4-3\beta) + \frac{\beta}{\gamma - 1}\right], \quad U_T = \frac{p}{u}\left(\frac{4-3\beta}{\Gamma_3 - 1}\right), \tag{135}$$

where $u/p = \beta/(\gamma - 1) + 3(1 - \beta)$. By substituting equations in Eq. (135) into Eqs. (102), (108) and (110), we can calculate the coefficients P_k, H_k, η_k and T_k ($k = r$, u and ℓ). Then, the derivatives du^r/dr, $d\ell/dr$ and dT/dr are obtained and numerically solved in order to calculate the transonic solutions for the adiabatic accretion disks. In Fig. 9, we show the sample transonic solutions of the adiabatic accretion disks with the black hole mass $M_{\rm BH} = 10 M_\odot$ and the mass accretion rate $\dot{M} = 10\dot{M}_{\rm Edd}$ where $\dot{M}_{\rm Edd} = 1.4 \times 10^{17}(M_{\rm BH}/M_\odot)$ [g s^{-1}] is the Eddington mass accretion rate. Sample solutions are calculated for $a/m = 0.0$, 0.5, 0.95 and 0.998 with dimensionless temperature $T_s = 0.05$, 0.01, 0.05 and 0.2, respectively. In Fig. 9, the radial component of four velocity u^r (*left panel*) and the dimensional temperature T [K] (*right panel*) are plotted. The positions of the horizons and the sonic points are denoted by the blank circles and filled triangles, respectively. The solutions are calculated so as to satisfy zero shear stress at the horizon. The temperatures of all solutions become smaller by several order inside the marginally stable orbit. This feature is same as the standard accretion disks. On the other hand, inside the marginally stable orbit, the absolute value of the radial component of the four velocity become large. This is because the

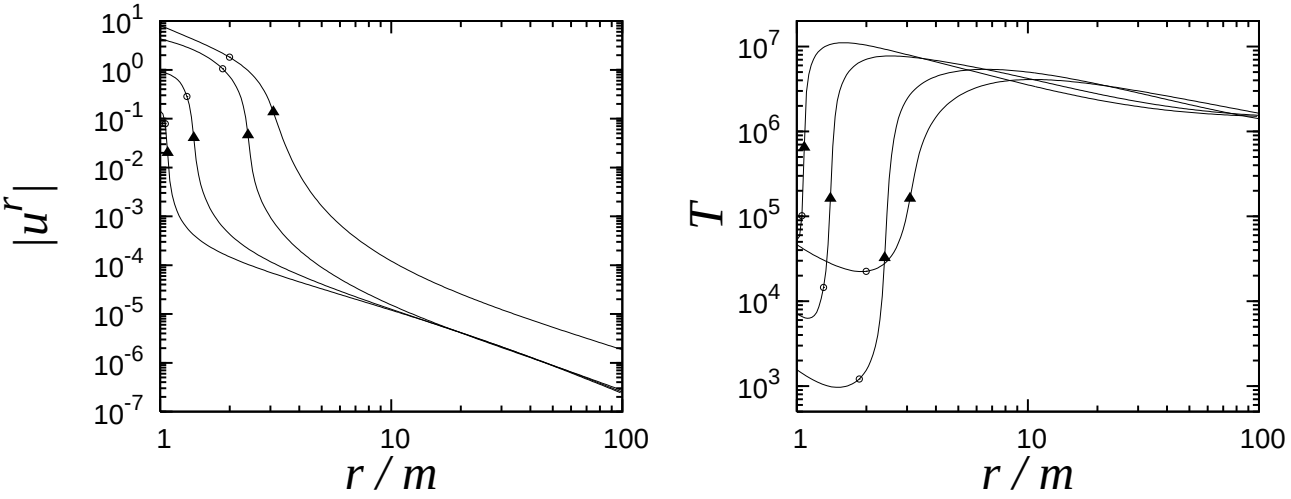

Figure 9. Sample numerical solutions for the adiabatic accretion disks when $a/m = 0.0$, 0.5, 0.95 and 0.998 with dimensionless temperature $T_s = 0.05$, 0.01, 0.05 and 0.2, respectively. The black hole mass $M_{\rm BH} = 10M_\odot$ and the mass accretion rate $\dot{M} = 10\dot{M}_{\rm Edd}$ are assumed. The radial component of four velocity u^r and the dimensional temperature T [K] are plotted. The positions of the horizons and the sonic points are denoted by the blank circles and filled triangles, respectively. The solutions are calculated so as to satisfy zero shear stress at the horizon. Here, the alpha viscosity parameter 0.01 and type A viscosity are assumed.

accretion flow approach the free fall motion with angular momentum in this region and plunge into the black hole horizon with high value of the gamma factor.

7.5 Application 5: Supercritical Accretion Disk with Photon-trapping Effects

Based on the formulation described above, we also calculate the simplest version of the transonic solutions of the slim disk of the supercritical accretion flow where the mass accretion rate is larger than the super-Eddington mass accretion rate. In general, for the supercritical accretion disks, the assumption of adiabatic changes, $dS = 0$, is not valid because in the vicinity of a black hole the pressure gradient enhance the radial velocity of the flow and the advection term in the energy equation can not be neglected. In such case, the energy equation with the effects of advection cooling, the radiation cooling and the viscous heating should be solved. In addition, near the horizon, photons are trapped within matters and can not escape from the accretion flow, and the flow become advection dominated state. The past studies actually solve the transonic solutions of the supercritical accretion flow (e.g. Watarai et al. 2001, Watarai & Mineshige 2001, Shimura & Manmoto 2003) by assuming that the specific heat at the constant volume, c_V, is independent of the temperature. For supercritical accretion flow, the heat inertia can not be neglected (Beloborodov 1998) and the photon-trapping effects near the horizon is also important. For the Boyer-Lindquist coordinate which have the coordinate singularity at the horizon, Beloborodov (1998) and Shimura & Manmoto (2003) solve the transonic solutions based on the acausal viscosity prescription.

From here, we just show the formulation of the transonic solutions for the supercritical accretion flows with effects of the heat inertia and the photon trapping with the general form of the specific heat at the constant volume, i.e., here, we do not assume that the specific heat at the constant volume, c_V, is independent of the temperature. For such flows, the internal energy u is calculated as

$$u = p_g g(T) + 3p_r, \tag{136}$$

where $g(T)$ is the same function used in the calculations of the transonic solutions of ADAFs with relativistic equation of state described in the previous section. First, we roughly estimate the photon trapping effects around black holes. In the optically thick region for photons in the supercritical accretion flows, the photons can escape from the disk surface after the diffusive processes in the disk. This holds only when the radiative diffusion timescale is shorter than the accretion timescale (see e.g. Katz 1977, Begelman 1978, Ohsuga et al. 2002, Kawaguchi 2003). The diffusion velocity is roughly calculated as $v_{\rm diff} \sim c/(3\tau)$. Then, the diffusion timescale of photons produced at equatorial plane is written as $t_{\rm diff} = H/v_{\rm diff}$. On the other hand, the accretion time scale is $t_{\rm acc} = r/(-u^r)$. When $t_{\rm diff} > t_{\rm acc}$, photons are trapped in the accretion disk and plunged into black hole without escaping from the disk surface. From the condition $t_{\rm diff} > t_{\rm acc}$, we can derive the photon-trapping radius, $r^*_{\rm trap}$, within which the parts of photons begin to be trapped as $r^*_{\rm trap} = [3\bar{\kappa}/(2\pi c)]H_\theta \dot{M}$ where $\bar{\kappa}$ is the mean opacity for photons. The radiation term including effects of the photon-trapping, the electron scattering and the free-free absorption is calculated as $q^-_{\rm rad} = f_{\rm trap} q^-_{\rm rad,0}$ where $q^-_{\rm rad,0}$ is the cooling rates when no effects of photon trapping. Now, $f_{\rm trap} = 1$ means no photon trapping and $f_{\rm trap} = 0$ means complete photon trapping. In this study, we assume $f_{\rm trap} = 1$ for $r > r_{\rm trap}$, but $f_{\rm trap} = 0$

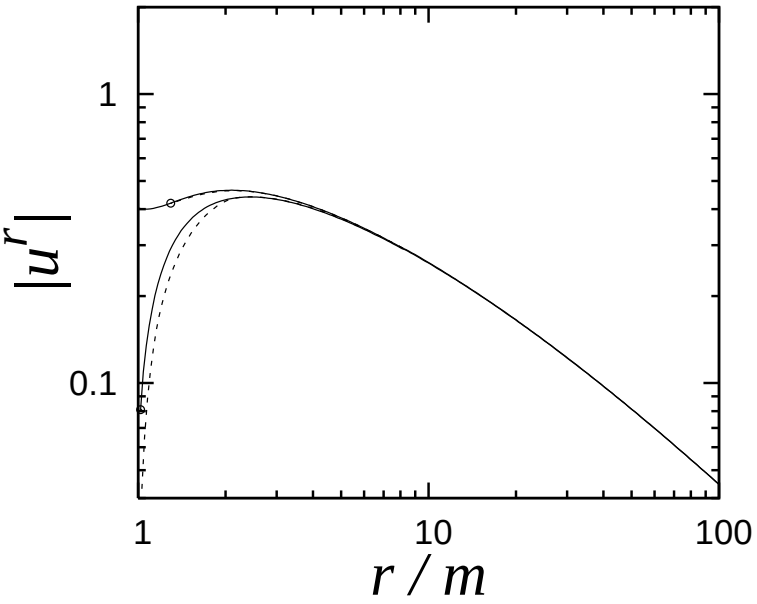

Figure 10. Transonic solutions of ADAF calculated by using the Kerr-Schild coordinate (*silid lines*) and the Boyer-Lindquist coordinate (*dashed lines*) for $a/m = 0.95$ and 0.99999. The parameters are same as Fig. 8. The blank circles show the position of the horizon.

for $r \leqslant r_{\rm trap}$, for simplicity. The radiative cooling term, $q^-_{\rm rad,0}$ [erg cm^{-3} s^{-1}], without the photon trapping is calculated as $q^-_{\rm rad,0} = F^-/(2rH_\theta)$ where F^- [erg cm^{-2} s^{-1}] is the energy loss rate from the disk surface which is calculated by using the Rosseland approximation as $F^- = (16\sigma_{\rm SB}T^4)/(3\bar{\kappa}\rho_0 r H_\theta)$ in the outside region, and F^- is calculated by the free-free emission inside region (Beloborodov 1998). Here, $\sigma_{\rm SB}$ is the Stephan-Boltzmann constant. We can calculate the coefficients $q^\pm_k$ ($k = r$, u and ℓ) as

$$q^\pm_r = -2S\sigma_r - q^-_{\rm rad},\ q^\pm_u = -2S\sigma_u,\ q^\pm_\ell = -2S\sigma_\ell. \tag{137}$$

On the other hand, from the EOS given by Eqs. (127) and (128), we obtain

$$P_\rho = \beta,\quad P_T = 4 - 3\beta,\quad U_\rho = \frac{\beta g(T) p}{u},\quad U_T = \frac{p}{u}\left[\beta\left(g + T\frac{dg}{dT}\right) + 12(1-\beta)\right], \tag{138}$$

where $u/p = \beta g(T) + 3(1-\beta)$ and $dg/dt = 15(15T^2 + 24T + 8)/(15T^2 + 20T + 8)^2$. By substituting Eqs. (138) and (137) into Eqs. (102), (108) and (110), we can calculate the coefficients P_k, H_k, η_k and T_k ($k = r$, u and ℓ). Then, the derivatives du^r/dr, $d\ell/dr$ and dT/dr are obtained and numerically solved in order to calculate the transonic solutions for the supercritical accretion disks with effects of advection cooling.

8 CONCLUDING REMARKS

Before summing up the results of this study, it may be better to note the arguments about the causality of the viscous flows at the event horizon. As already pointed out by Popham & Gammie (1998), the formalism of the causal viscosity prescription give the solutions with the finite values of the outward energy flux and the outward angular momentum at the horizon, and they stated that this property does not suggest the causality violation (Popham & Gammie 1998). If the viscosity is described by the fluctuations of the Maxwell stress and/or the Reynolds stress from the mean values such as the angular momentum transport by the magnetorotational instability (MRI), these fluctuating parts should be correctly treated in the general relativistic point of view which may require the extended causal thermodynamics such as the Israel-Stewart theory (Israel & Stewart 1979) where the causality violating infinite signal speeds are eliminated. The hydrodynamical equations based on such theory are formulated by Peitz & Appl (1998). If the extended causal thermodynamics for the magnetohydrodynamical flows can be used, the problems of the causality of the viscous flows at the event horizon will be clearly resolved in the future.

The another limitation of the viscosity prescription used in this paper is shown in Fig. 10. In this figure, we show the transonic solutions of ADAF calculated by using the Kerr-Schild coordinate (*silid lines*) and the Boyer-Lindquist coordinate (*dashed lines*) for $a/m = 0.95$ and 0.99999. The parameters are same as Fig. 8. For the case of $a/m = 0.95$, the two solutions have almost same results. For the cases of lower spin parameters than $a/m = 0.95$, the same solutions by using the two coordinate are obtained. However, in the case of $a/m = 0.99999$ shown in Fig. 10, the two results are not exactly same. This feature show that the viscosity prescription used in this paper is not perfectly coordinate invariant. When we introduce the

causality limited viscosity, we use some special frame in order to evaluate the physical quantities such as the shear stress S or the factor f_c. However, there is no guarantee that these physical quantities introduced in the specific reference frame have the invariant feature with respect to the coordinate transformation or the frame transformation. If we can define and introduce the invariant viscosity, the accretion flows calculated by the two procedures produce the same results such as the ideal flows. So, the viscous flows presented in the previous sections are not very exactly reproduced from the calculations based on the Boyer-Lindquist coordinate such as the past studies. The invariant viscosity prescription will be made by the extended causal thermodynamics stated above.

From here, we give the conclusions of the present study. In the present study, we give the basic equations and the calculation method for the horizon-penetrating transonic accretion disks or flows in the equatorial plane written by the Kerr-Schild coordinate where there is no coordinate singularity at the event horizon. Based on these formalism, we calculate the transonic solutions of these types of the accretion flow models from the outer region to inside region of the event horizon; the ideal isothermal flows, the ideal and the viscous polytropic flows, and the advection dominated accretion flows (ADAFs) with the relativistic equation of state, the adiabatic accretion disks, the standard accretion disks and the supercritical accretion disks. In this study, we use two types of the causal viscosity prescriptions. One is the simple treatment of the kinematic viscosity and the other is based on the shear stress measure in the FRF. When we use the causal viscosity prescription based on the shear stress measured in the FRF, the boundary condition for the transonic accretion flows is also given at the viscous point where the accreting radial velocity is nearly equal to the viscous diffusion velocity. By using the causal viscosity prescription, the ADAF transonic solutions are firstly obtained by Gammie & Popham (1998) for the general relativistic flows and later for the pseudo-Newtonian flows (Takahashi 2007).

Based on the solutions obtained in the present study, we calculate the physical values for the transonic solutions of the these disks around the rotating black hole just on the event horizon and inside the horizon. These solutions are obtained for both non-rotating and rotating black holes. In general, the accretion flows calculated by using the Kerr-Schild coordinate plunge into black hole with finite three velocity smaller than the speed of light even at the event horizon or inside the horizon, and the angular velocities at the horizon are different from the angular velocity of the frame-dragging due to the black hole's rotation. These features are different from the results obtained by using the Boyer-Lindquist coordinate with the coordinate singularity at the horizon.

By using the formalism presented in the present study and adding the required physics, we can basically calculate the another types of more realistic accretion flows including the radiatively inefficient accretion flows (RIAF) in the galactic center, the supercritical accretion disks which is sometimes assumed in the center of the black-hole X-ray binaries or Syfert galaxies, and the hypercritical accretion flows or the neutrino-dominated accretion flows (NDAFs) in gamma-ray burst. Also, by using the formulations and the calculation methods in this study, the accretion flows inside the black hole satisfying the boundary conditions outside the black hole can be calculated. Although the accretion flow structure inside the event horizon can not be seen directly by the observer outside the event horizon, by combining the constraints obtained by the future observations for the regions just outside the event horizon of the black hole candidate such as the massive black hole at the galactic center with the theoretical calculations such as this study or more sophysticated study inside the black hole, we can know the accretion flow structure inside the event horizon of the black hole in the real world in the future. Especially, by the near-future observations by the radio interferometer such as e.g. VSOP-2 for radio (Hirabayashi et al. 2005), MAXIM for soft X-ray (see MAXIM web page: http://maxim.gsfc.nasa.gov/), the direct-mapping of the black hole shadow in the RIAF in the galactic center will be performed (e.g. Falcke et al. 2000; Melia & Falcke 2001 for review, Melia 2003a, 2003b and references therein) and give the information of the strong-gravity region as the resolved images around the shadow. It is known that such images will give the physical information of the black hole itself or the accretion flows in the strong-gravity region (e.g. Cunningham & Bardeen 1972, 1973, Bardeen 1973, Takahashi 2004, 2005, Broderick & Loeb 2005, 2006, Broderick & Narayan 2006, Zakharov et al. 2005, Yuan et al. 2006) . However, so far, the image of the black hole shadows calculated by using the general relativistic transonic flows of the RIAF have not been performed. Our calculations presented in this study can be also applied to such calculations with the radiation mechanisms and the required physics.

ACKNOWLEDGMENTS

The author is grateful to Professors Y. Eriguchi and S. Mineshige for their continuous encouragements, and K. Watarai, S. Mineshige, K. Ohsuga, M. Takahashi, K. Nakao, S. Nagataki, J. Fukue, R. Matsumoto, N. Kawanaka, Y. Sekiguchi, M. Shibata, T. Yamamoto and A. Yoshinaga for useful discussion and comments. The author also thanks the anonymous referee for helpful and useful comments. This research was partially supported by the Ministry of Education, Culture, Sports, Science and Technology, Grant-in-Aid for Japan Society for the Promotion of Science (JSPS) Fellows (17010519).

REFERENCES

Abramowicz, M. A., Chen, X., Granath, M., & Lasota, J.-P., 1997, ApJ, 471, 762
Abramowicz, M. A., Lanza, A., & Percival, M. J., 1997, ApJ, 479, 179
Bardeen, J. M., 1970, ApJ, 162, 71
Bardeen, J.M., 1973, in Black Holes, ed. C. DeWitt and B. DeWitt (Gordon and Breach, New York)
Bardeen, J. M., Press, W. H., Teukolsky, S. A., 1972, ApJ, 178, 347
Begelman, M. C., 1978, MNRAS, 184, 53
Beloborodov, A. M., 1998, MNRAS, 297, 739
Beloborodov, A. M., Abramowicz, M. A., Novikov, I. D., 1997, ApJ, 419, 267
Broderick, A. E., Loeb, A., 2005, MNRAS, 363, 353
Broderick, A. E., Loeb, A., 2006, ApJ, 636, L109
Broderick, A. E., Narayan, R., 2006, ApJ, 638, L21
Chakrabarti, S., 1996, ApJ, 471, 237
Chandrasekhar, S., 1939, An Introduction to the Study of Stellar Structure
Cook, G. B., 2000, Max-Planck-Gesellschaft Living Reviews Series, No. 2000-5
Cox, J. P., Giuli, R. T., 1968, Principles of Stellar Structure, Vol. 2 (Gordon and Breach, New York)
Cunningham, C. T., Bardeen, J. M., 1972, ApJ, 173, 137
Cunningham, C. T., Bardeen, J. M., 1973, ApJ, 183, 237
Falcke, H., Melia, F., Agol, E., 2000, ApJ, 528, L13
Font, J. A., Ibáñez, J. M., Papadopoulos, P., 1998, ApJ, 507, 67
Font, J. A., Ibáñez, J. M., Papadopoulos, P., 1999, MNRAS, 305, 920
Font, J. A., 2000, Max-Planck-Gesellschaft Living Reviews Series, No. 2000-2
Frolov, V. P., Novikov, I. D., 1998, Black Hole Physics: Basic Concepts and New Developments, Kluwer Academic
Fukue, J., 1987, PASJ, 39, 309
Gammie, C. F., McKinney, J. C., Tóth, G., 2003, ApJ, 598, 444
Gammie, C. F., Shapiro, S. L., McKinney, J. C., 2004, ApJ, 602, 312
Gammie, C., & Popham, R., 1998, ApJ, 498, 313
Hirabayashi, H., et al., 2005, in Proc. 7th Symp. European VLBI Network on New Developments in VLBI Science and Technology, ed. R. Bachiller, F. Colomer, J.-F. Desmars, & P. de Vicente (Obs. Astron. Nac. Spain), 285 (astro-ph/0501020)
Israel, W., & Stewart, J. M., 1979, Ann. Phys., 118, 341
Jaroszyski, M., & Kurpiewski, A. 1997, A&A, 326, 419
Katz, J. I., 1977, ApJ, 215, 265
Kawaguchi, T., 2003, ApJ, 593, 69
Komissarov, S. S., 2001, MNRAS, 326, L41
Komissarov, S. S., 2004, MNRAS, 350, 1431
Matsumoto, R., Kato, S., Fukue, J., Okazaki, A. T., 1984, PASJ, 36, 71
Manmoto, T., 2000, ApJ, 534, 734
Melia, F., Falcke, H., 2001, ARA& A, 39, 309
Melia, F., 2003a, The black hole at the center of our galaxy, Princeton University Press
Melia, F., 2003b, The edge of infinity, Supermassive Black Holes in the Universe, Cambridge University Press
Misner, C. W., Thorne, K. S., & Wheeler, J. A. 1973, Gravitation, Freeman
Narayan, R., 1992, ApJ, 394, 261
Narayan, R., Kato, S., & Honma, F., 1997, ApJ, 476, 49
Novikov, I. D., & Thorne, K. S., 1973, in Black Holes, ed. C. DeWitt and B. DeWitt (Gordon and Breach, New York)
Ohsuga, K., Mineshige, S., Mori, M., Umemura, M., 2002, ApJ, 574, 315
Page, D., & Thorne, K. S., 1974, ApJ, 191, 499
Papadopoulos, P., & Font, J. A., 1998, Phys. Rev. D, 58, 024005
Papaloizou, J. C. B., & Szuszkiewicz, E., 1994, MNRAS, 268, 29
Peitz, J., & Appl, S., 1997, MNRAS, 286, 681
Peitz, J., & Appl, S., 1997, MNRAS, 296, 231
Popham, R., & Gammie, C., 1998, ApJ, 504, 419
Popham, R., Woosley, S. E., & Fryer, C., 1999, ApJ, 518, 356
Shakura, N. I., & Sunyaev, R. A., 1973, A& A, 24, 337
Shimura, T., & Manmoto, T., 2003, MNRAS, 338, 1013
Takahashi, R., 2004, ApJ, 611, 996
Takahashi, R., 2005, PASJ, 57, 273

Takahashi, R., 2007, A& A, 461, 393
Watarai, K., Fukue, J., Takeuchi, M., Mineshige, S., 2000, PASJ, 52, 133
Watarai, K., Mineshige, S., 2001, PASJ, 53, 915
Yuan, F., Shen, Z.-Q., Huang, L., 2006, 642, L45
Zakharov, A. F., de Paolis, F., Ingrosso, G., Nucita, A. A., 2005, A&A, 442, 795

APPENDIX A: METRIC COMPONENTS

The components of $g_{\mu\nu}$ and $g^{\mu\nu}$ are calculated as

$$g_{\mu\nu} = \begin{pmatrix} -\alpha^2 + \beta^k\beta_k & \beta_i \\ \beta_i & \gamma_{ij} \end{pmatrix}, \tag{A1}$$

and

$$g^{\mu\nu} = \begin{pmatrix} -1/\alpha^2 & \beta^i/\alpha^2 \\ \beta^i/\alpha^2 & \gamma^{ij} - \beta^i\beta^j/\alpha^2 \end{pmatrix}. \tag{A2}$$

The explicit forms of the non-zero components of $g_{\mu\nu}$ and $g^{\mu\nu}$ are calculated as

$$\begin{aligned} g_{tt} &= -\left(1 - \frac{2mr}{\Sigma}\right), \quad g_{tr} = g_{rt} = \frac{2mr}{\Sigma}, \quad g_{t\phi} = g_{\phi t} = -\frac{2mar\sin^2\theta}{\Sigma}, \quad g_{rr} = 1 + \frac{2mr}{\Sigma}, \\ g_{r\phi} &= g_{\phi r} = -a\sin^2\theta\left(1 + \frac{2mr}{\Sigma}\right), \quad g_{\theta\theta} = \Sigma, \quad g_{\phi\phi} = \frac{A\sin^2\theta}{\Sigma}, \end{aligned} \tag{A3}$$

and

$$g^{tt} = -\left(1 + \frac{2mr}{\Sigma}\right), \quad g^{tr} = g^{rt} = \frac{2mr}{\Sigma}, \quad g^{rr} = \frac{\Delta}{\Sigma}, \quad g^{r\phi} = g^{\phi r} = \frac{a}{\Sigma}, \quad g^{\theta\theta} = \frac{1}{\Sigma}, \quad g^{\phi\phi} = \frac{1}{\Sigma\sin^2\theta}, \tag{A4}$$

where nonzero components of β_i and γ^{ij} are

$$\beta_r = g_{tr} = \frac{2mr}{\Sigma}, \quad \beta_\phi = g_{t\phi} = -\frac{2mar\sin^2\theta}{\Sigma}, \quad \gamma^{rr} = \frac{A}{\Sigma(\Sigma + 2mr)}, \quad \gamma^{r\phi} = \gamma^{\phi r} = \frac{a}{\Sigma}, \quad \gamma^{\theta\theta} = \frac{1}{\Sigma}, \quad \gamma^{\phi\phi} = \frac{1}{\Sigma\sin^2\theta}.$$

Here, we use $\beta_i = \gamma_{ij}\beta^j$ and $\gamma^{ik}\gamma_{kj} = \delta^i_j$ where δ^i_j represents the Kronekker delta.

APPENDIX B: CONGRUENCES FOR THE OBSERVER DRAGGING WITH THE BLACK HOLE'S ROTATION

Here, we show that the congruences for the observer rotating with the angular velocity of the frame-dragging written by the Kerr-Schild coordinate have the singularity at the event horizon. We consider the observer rotating with the angular velocity, $\omega = 2mar/A$, which is the angular velocity of the frame dragging due to the black hole's rotation. For such observer, by using the normalization condition $u^\mu u_\mu = -1$, the contravariant components of the four velocity are described as

$$u^t = \left(\frac{\Delta\Sigma}{A}\right)^{1/2}, \quad u^r = u^\theta = 0, \quad u^\phi = \omega u^t. \tag{B1}$$

Since $\Delta < 0$, $\Sigma > 0$ and $A > 0$ within the event horizon, the component u^t become imaginary. Then, in this study, the congruences for the observer moving with are not used when the transformation of the physical quantities between the KSF and the FRF.

APPENDIX C: TRANSFORMATION BETWEEN THE KERR-SCHILD FRAME AND THE FLUID'S REST FRAME BY TETRADS

First, we give the tetrad components connecting the KSF and the LNRF made by the congruences of the observer with $u_\mu = -\alpha\delta^t_\mu$. For such congruences, we have $u^t = \alpha^{-1}$ and $u^k = -\alpha^{-1}\beta^k$ ($k = r,\ \theta,\ \phi$). According with such congruences, the metric can be expressed as

$$ds^2 = -\alpha^2 dt^2 + \frac{1}{\gamma^{rr}}\left(dr + \beta^r dt\right)^2 + \gamma_{\theta\theta}d\theta^2 + \gamma_{\phi\phi}\left[d\phi + \frac{\gamma_{r\phi}}{\gamma_{\phi\phi}}\left(dr + \beta^r dt\right)\right]^2, \tag{C1}$$

$$= -\left(\frac{\Sigma}{\Sigma + 2mr}\right)dt^2 + \frac{\Sigma(\Sigma + 2mr)}{A}\left(dr + \frac{2mr}{\Sigma + 2mr}dt\right)^2 + \Sigma d\theta^2 + \frac{A\sin^2\theta}{\Sigma}\left[d\phi - \omega dt - \frac{a}{A}(\Sigma + 2mr)dr\right]^2, \tag{C2}$$

where we use $\gamma^{rr} = \gamma_{\phi\phi}/(\gamma_{rr}\gamma_{\phi\phi} - \gamma_{r\phi}^2)$. By using the tetrad transformation $x^{\hat{\nu}} = e_{\mu}{}^{\hat{\nu}} x^{\mu}$ where the hat denote the components measured in the LNRF having the orthonormal tetrad basis, the metric can be calculated as

$$ds^2 = -\left[e_{\mu}{}^{\hat{t}} dx^{\mu}\right]^2 + \left[e_{\mu}{}^{\hat{r}} dx^{\mu}\right]^2 + \left[e_{\mu}{}^{\hat{\theta}} dx^{\mu}\right]^2 + \left[e_{\mu}{}^{\hat{\phi}} dx^{\mu}\right]^2 . \tag{C3}$$

Then, the components of the tetrad $e_{\mu}{}^{\hat{\nu}}$ connecting between the KSF and the LNRF are calculated as,

$$\begin{pmatrix} e_t{}^{\hat{t}} & e_t{}^{\hat{r}} & e_t{}^{\hat{\theta}} & e_t{}^{\hat{\phi}} \\ e_r{}^{\hat{t}} & e_r{}^{\hat{r}} & e_r{}^{\hat{\theta}} & e_r{}^{\hat{\phi}} \\ e_\theta{}^{\hat{t}} & e_\theta{}^{\hat{r}} & e_\theta{}^{\hat{\theta}} & e_\theta{}^{\hat{\phi}} \\ e_\phi{}^{\hat{t}} & e_\phi{}^{\hat{r}} & e_\phi{}^{\hat{\theta}} & e_\phi{}^{\hat{\phi}} \end{pmatrix} = \begin{pmatrix} \alpha & \beta^r(\gamma^{rr})^{-1/2} & 0 & \beta^r\gamma_{r\phi}(\gamma_{\phi\phi})^{-1/2} \\ 0 & (\gamma^{rr})^{-1/2} & 0 & \gamma_{r\phi}(\gamma_{\phi\phi})^{-1/2} \\ 0 & 0 & (\gamma_{\theta\theta})^{1/2} & 0 \\ 0 & 0 & 0 & (\gamma_{\phi\phi})^{1/2} \end{pmatrix} \tag{C4}$$

$$= \begin{pmatrix} \left(\frac{\Sigma}{\Sigma+2mr}\right)^{1/2} & \frac{2mr}{A^{1/2}}\left(\frac{\Sigma}{\Sigma+2mr}\right)^{1/2} & 0 & -\frac{2mra\sin\theta}{(\Sigma A)^{1/2}} \\ 0 & \left[\frac{\Sigma(\Sigma+2mr)}{A}\right]^{1/2} & 0 & -\frac{a\sin\theta(\Sigma+2mr)}{(A\Sigma)^{1/2}} \\ 0 & 0 & \Sigma^{1/2} & 0 \\ 0 & 0 & 0 & \sin\theta\left(\frac{A}{\Sigma}\right)^{1/2} \end{pmatrix} . \tag{C5}$$

By using $e^{\mu\hat{\nu}} = g^{\mu\lambda} e_{\lambda}{}^{\hat{\nu}}$ and $e^{\mu}{}_{\hat{\nu}} = \eta_{\hat{\nu}\hat{\lambda}} e^{\mu\hat{\lambda}}$ where $(\eta_{\hat{\mu}\hat{\nu}})$ is the metric of the Lorentz frame, i.e. $\mathrm{diag}(\eta_{\hat{\mu}\hat{\nu}}) = (-1,1,1,1)$ and the non-diagonal components of $\eta_{\hat{\mu}\hat{\nu}}$ are null, we also have the components for the tetrad $e^{\mu}{}_{\hat{\nu}}$ calculated as

$$\begin{pmatrix} e^t{}_{\hat{t}} & e^t{}_{\hat{r}} & e^t{}_{\hat{\theta}} & e^t{}_{\hat{\phi}} \\ e^r{}_{\hat{t}} & e^r{}_{\hat{r}} & e^r{}_{\hat{\theta}} & e^r{}_{\hat{\phi}} \\ e^\theta{}_{\hat{t}} & e^\theta{}_{\hat{r}} & e^\theta{}_{\hat{\theta}} & e^\theta{}_{\hat{\phi}} \\ e^\phi{}_{\hat{t}} & e^\phi{}_{\hat{r}} & e^\phi{}_{\hat{\theta}} & e^\phi{}_{\hat{\phi}} \end{pmatrix} = \begin{pmatrix} \alpha^{-1} & 0 & 0 & 0 \\ -\beta^r\alpha^{-1} & (\gamma^{rr})^{1/2} & 0 & 0 \\ 0 & 0 & (\gamma^{\theta\theta})^{1/2} & 0 \\ 0 & \gamma^{r\phi}(\gamma^{rr})^{-1/2} & 0 & (\gamma_{\phi\phi})^{-1/2} \end{pmatrix} \tag{C6}$$

$$= \begin{pmatrix} \left(\frac{\Sigma+2mr}{\Sigma}\right)^{1/2} & 0 & 0 & 0 \\ \frac{-2mr}{[\Sigma(\Sigma+2mr)]^{1/2}} & \left[\frac{A}{\Sigma(\Sigma+2mr)}\right]^{1/2} & 0 & 0 \\ 0 & 0 & \frac{1}{\Sigma^{1/2}} & 0 \\ 0 & a\left(\frac{\Sigma+2mr}{\Sigma A}\right)^{1/2} & 0 & \frac{1}{\sin\theta}\left(\frac{\Sigma}{A}\right)^{1/2} \end{pmatrix} . \tag{C7}$$

Since we now consider the accretion flows in the equatorial plane, we assume that the physical quantities measured in the LNRF are transformed to the physical quantities measured in the FRF by two-dimensional Lorentz transformation with the radial velocity $\hat{v}_r$ and the azimuthal velocity $\hat{v}_\phi$. Here, we assume that the FRF moves with the radial velocity $\hat{v}_r$ and the azimuthal velocity $\hat{v}_\phi$ with respect to the LNRF. Inversely, the LNRF moves with the radial velocity $-\hat{v}_r$ and the azimuthal velocity $-\hat{v}_\phi$ with respect to the FRF. The tetrads $e_{\hat{\nu}}{}^{(\lambda)}$ and $e^{\hat{\nu}}{}_{(\lambda)}$ connecting between the LNRF and the FRF are two-dimensional Lorentz transformation with the radial velocity $\hat{v}_r$ and the azimuthal velocity $\hat{v}_\phi$ measured in the LNRF. The transformation matrix $e^{\hat{\nu}}{}_{(\lambda)}$ are described as

$$\begin{pmatrix} e^{\hat{t}}{}_{(t)} & e^{\hat{t}}{}_{(r)} & e^{\hat{t}}{}_{(\theta)} & e^{\hat{t}}{}_{(\phi)} \\ e^{\hat{r}}{}_{(t)} & e^{\hat{r}}{}_{(r)} & e^{\hat{r}}{}_{(\theta)} & e^{\hat{r}}{}_{(\phi)} \\ e^{\hat{\theta}}{}_{(t)} & e^{\hat{\theta}}{}_{(r)} & e^{\hat{\theta}}{}_{(\theta)} & e^{\hat{\theta}}{}_{(\phi)} \\ e^{\hat{\phi}}{}_{(t)} & e^{\hat{\phi}}{}_{(r)} & e^{\hat{\phi}}{}_{(\theta)} & e^{\hat{\phi}}{}_{(\phi)} \end{pmatrix} = \begin{pmatrix} \hat{\gamma} & \hat{\gamma}\hat{v}_r & 0 & \hat{\gamma}\hat{v}_\phi \\ \hat{\gamma}\hat{v}_r & 1+\frac{\hat{\gamma}^2\hat{v}_r^2}{1+\hat{\gamma}} & 0 & \frac{\hat{\gamma}^2\hat{v}_r\hat{v}_\phi}{1+\hat{\gamma}} \\ 0 & 0 & 1 & 0 \\ \hat{\gamma}\hat{v}_\phi & \frac{\hat{\gamma}^2\hat{v}_r\hat{v}_\phi}{1+\hat{\gamma}} & 0 & 1+\frac{\hat{\gamma}^2\hat{v}_\phi^2}{1+\hat{\gamma}} \end{pmatrix} \tag{C8}$$

where $\hat{\gamma} = (1 - \hat{v}_r^2 - \hat{v}_\phi^2)^{-1/2}$. Since both the LNRF and the FRF are orthonormal, the transformation matrix $e_{\hat{\nu}}{}^{(\lambda)}$ are calculated as

$$\begin{pmatrix} e_{\hat{t}}{}^{(t)} & e_{\hat{t}}{}^{(r)} & e_{\hat{t}}{}^{(\theta)} & e_{\hat{t}}{}^{(\phi)} \\ e_{\hat{r}}{}^{(t)} & e_{\hat{r}}{}^{(r)} & e_{\hat{r}}{}^{(\theta)} & e_{\hat{r}}{}^{(\phi)} \\ e_{\hat{\theta}}{}^{(t)} & e_{\hat{\theta}}{}^{(r)} & e_{\hat{\theta}}{}^{(\theta)} & e_{\hat{\theta}}{}^{(\phi)} \\ e_{\hat{\phi}}{}^{(t)} & e_{\hat{\phi}}{}^{(r)} & e_{\hat{\phi}}{}^{(\theta)} & e_{\hat{\phi}}{}^{(\phi)} \end{pmatrix} = \begin{pmatrix} e^{\hat{t}}{}_{(t)} & -e^{\hat{t}}{}_{(r)} & -e^{\hat{t}}{}_{(\theta)} & -e^{\hat{t}}{}_{(\phi)} \\ -e^{\hat{r}}{}_{(t)} & e^{\hat{r}}{}_{(r)} & e^{\hat{r}}{}_{(\theta)} & e^{\hat{r}}{}_{(\phi)} \\ -e^{\hat{\theta}}{}_{(t)} & e^{\hat{\theta}}{}_{(r)} & e^{\hat{\theta}}{}_{(\theta)} & e^{\hat{\theta}}{}_{(\phi)} \\ -e^{\hat{\phi}}{}_{(t)} & e^{\hat{\phi}}{}_{(r)} & e^{\hat{\phi}}{}_{(\theta)} & e^{\hat{\phi}}{}_{(\phi)} \end{pmatrix} . \tag{C9}$$

Since now we have both the tetrads between the KSF and the LNRF and the tetrad between the LNRF and the KSF, the tetrad connecting the KSF and the FRF, e.g. $e^{\mu}{}_{(\nu)}$ and $e_{\mu}{}^{(\nu)}$, are calculated as

$$e^{\mu}{}_{(\nu)} = e^{\mu}{}_{\hat{\lambda}} e^{\hat{\lambda}}{}_{(\nu)}, \quad e_{\mu}{}^{(\nu)} = e_{\mu}{}^{\hat{\lambda}} e_{\hat{\lambda}}{}^{(\nu)}. \tag{C10}$$

By using these tetrad, we can transform the physical quantities between the KSF and the FRF as

$$u^{\mu} = e^{\mu}{}_{(\nu)} u^{(\nu)}, \quad u_{\mu} = e_{\mu}{}^{(\nu)} u_{(\nu)}, \tag{C11}$$

$$t^{\mu\nu} = e^{\mu}{}_{(\lambda)} e^{\nu}{}_{(\xi)} t^{(\lambda)(\xi)}, \quad t_{\mu\nu} = e_{\mu}{}^{(\lambda)} e_{\nu}{}^{(\xi)} t_{(\lambda)(\xi)}, \quad t^{\mu}{}_{\nu} = e^{\mu(\lambda)} e_{\nu}{}^{(\xi)} t_{(\lambda)(\xi)}, \tag{C12}$$

and so on. Lowering and raising the index μ of the tetrads are done by $g_{\mu\nu}$ and $g^{\mu\nu}$. On the other hand, lowering and raising the index μ of the tetrads are done by $\eta_{(\mu)(\nu)}$ and $\eta^{(\mu)(\nu)}$ which are the metric of the Lorentz frame.

APPENDIX D: VELOCITY FIELDS

By using the tetrads derived in Appendix C, in this appendix, we first derive the velocity fields u^{μ} and u_{μ} in the KSF described by the radial velocity $\hat{v}_r$ and the azimuthal velocity $\hat{v}_{\phi}$ of the FRF with respect to the LNRF. Since $u^{(t)} = -u_{(t)} = 1$ and $u^{(k)} = u_{(k)} = 0$ $(k = r,\ \theta,\ \phi)$, the four velocity is calculated as $u^{\mu} = e^{\mu}{}_{(\nu)} u^{(\nu)} = e^{\mu}{}_{(t)} u^{(t)} = e^{\mu}{}_{(t)} = e^{\mu}{}_{\hat{\lambda}} e^{\hat{\lambda}}{}_{(t)}$ and $u_{\mu} = e_{\mu}{}^{(\nu)} u_{(\nu)} = e_{\mu}{}^{(t)} u_{(t)} = -e_{\mu}{}^{(t)} = -e_{\mu}{}^{\hat{\lambda}} e_{\hat{\lambda}}{}^{(t)}$. Then, we have

$$\begin{pmatrix} u^t \\ u^r \\ u^{\theta} \\ u^{\phi} \end{pmatrix} = \begin{pmatrix} \alpha^{-1}\hat{\gamma} \\ -\beta^r \alpha^{-1}\hat{\gamma} + (\gamma^{rr})^{1/2}\hat{\gamma}\hat{v}_r \\ 0 \\ \gamma^{r\phi}(\gamma^{rr})^{-1/2}\hat{\gamma}\hat{v}_r + (\gamma_{\phi\phi})^{-1/2}\hat{\gamma}\hat{v}_{\phi} \end{pmatrix}, \tag{D1}$$

and

$$\begin{pmatrix} u_t \\ u_r \\ u_{\theta} \\ u_{\phi} \end{pmatrix} = \begin{pmatrix} -\alpha\hat{\gamma} + \beta^r(\gamma^{rr})^{-1/2}\hat{\gamma}\hat{v}_r + \beta^r\gamma_{r\phi}(\gamma_{\phi\phi})^{-1/2}\hat{\gamma}\hat{v}_{\phi} \\ (\gamma^{rr})^{-1/2}\hat{\gamma}\hat{v}_r + \gamma_{r\phi}(\gamma_{\phi\phi})^{-1/2}\hat{\gamma}\hat{v}_{\phi} \\ 0 \\ (\gamma_{\phi\phi})^{1/2}\hat{\gamma}\hat{v}_{\phi} \end{pmatrix}. \tag{D2}$$

From u^t, u^r and $u_{\phi}(= \ell)$, we can derive Eq. (7) as

$$\hat{v}_r = \frac{u^r + \beta^r u^t}{\hat{\gamma}(\gamma_{rr})^{1/2}} = \frac{\Sigma + 2mr}{u^t A^{1/2}} \left(u^r + \frac{2mr}{\Sigma + 2mr} u^t \right), \quad \hat{v}_{\phi} = \frac{\ell}{\hat{\gamma}(\gamma_{\phi\phi})^{1/2}} = \frac{\ell}{u^t} \left(\frac{\Sigma + 2mr}{A} \right)^{1/2}, \tag{D3}$$

where we use $\theta = \pi/2$.

APPENDIX E: SHEAR RATE

In this appendix, we calculate the coefficients σ_r, σ_u and σ_{ℓ} which gives the shear rate $\sigma(\equiv \sigma_{(r)(\phi)})$ measured in the FRF by

$$\sigma = \sigma_r + \sigma_u \frac{du^r}{dr} + \sigma_{\ell} \frac{d\ell}{dr}.$$

The shear rate $\sigma_{(r)(\phi)}$ in the FRF is calculated from the shear rate $\sigma_{\mu\nu}$ in the KSF as $\sigma_{(r)(\phi)} = e^{\mu}{}_{(r)} e^{\nu}{}_{(\phi)} \sigma_{\mu\nu}$. Here, non-zero components of the tetrads are $e^{\mu}{}_{(r)}$ $(\mu = t,\ r,\ \phi)$ and $e^{\nu}{}_{(\phi)}$ $(\nu = t,\ r,\ \phi)$ which can be calculated by the tetrad connecting the KSF and the LNRF, $e^{\mu}{}_{\hat{\lambda}}$, and the tetrad connecting the LNRF and the FRF, $e^{\hat{\lambda}}{}_{(\alpha)}$ $(\alpha = r,\ \phi)$ given in Appendix C. Since $\sigma_{\mu\nu} = \sigma_{\nu\mu}$, we need to calculate six components of the shear rate, i.e. σ_{tt}, σ_{tr}, $\sigma_{t\phi}$, σ_{rr}, $\sigma_{r\phi}$ and $\sigma_{\phi\phi}$. The shear rate $\sigma_{\mu\nu}$ is calculated as the traceless part of the deformation tensor which is calculated as $\sigma_{\mu\nu} = (u_{\mu;\alpha} h^{\alpha}_{\nu} + u_{\nu;\alpha} h^{\alpha}_{\mu})/2 - \Theta h_{\mu\nu}/3$. We give the covariant derivative for u_{μ} and the four acceleration a_{μ} which are directly used for the calculations of the shear rate $\sigma_{\mu\nu}$. The non-zero components of $u_{\mu;nu}$ are calculated as

$$\begin{aligned}
&u_{t;t} = \frac{1}{2} g_{tt,r} u^r, \quad u_{r;t} = -\frac{1}{2}(g_{tt,r} + \Omega g_{t\phi,r}) u^t, \quad u_{\phi;t} = \frac{1}{2} g_{t\phi,r} u^r, \quad u_{t;r} = -\frac{d\mathcal{E}}{dr} - \frac{1}{2}(g_{tt,r} + \Omega g_{t\phi,r}) u^t, \\
&u_{r;r} = \frac{du_r}{dr} - \frac{1}{2} g_{rr,r} u^r - (g_{tr,r} + \Omega g_{r\phi,r}) u^t, \quad u_{\phi;r} = \frac{d\ell}{dr} - \frac{1}{2}(g_{t\phi,r} + \Omega g_{\phi\phi,r}) u^t, \quad u_{\theta;\theta} = \frac{1}{2} g_{\theta\theta,r} u^r, \\
&u_{t;\phi} = \frac{1}{2} g_{t\phi,r} u^r, \quad u_{r;\phi} = -\frac{1}{2}(g_{t\phi,r} + \Omega g_{\phi\phi,r}) u^t, \quad u_{\phi;\phi} = \frac{1}{2} g_{\phi\phi,r} u^r.
\end{aligned} \tag{E1}$$

The covariant components of the four acceleration, $a_{\mu} = u_{\mu;\nu} u^{\nu}$, are calculated as

$$a_t = -u^r \frac{d\mathcal{E}}{dr}, \quad a_r = u^r \frac{du_r}{dr} - \frac{1}{2} g_{rr,r} (u^r)^2 - (g_{tr,r} + g_{r\phi,r}\Omega) u^t u^r - \frac{1}{2}(u^t)^2 g_{\phi\phi,r} (\Omega - \Omega^+_K)(\Omega - \Omega^-_K), \quad a_{\theta} = 0, \quad a_{\phi} = u^r \frac{d\ell}{dr}. \tag{E2}$$

We next calculate the expansion $\Theta = u^{\gamma}{}_{;\gamma}$. The covariant derivatives $u^{t}{}_{;t}$, $u^{r}{}_{;r}$, $u^{\theta}{}_{;\theta}$ and $u^{\phi}{}_{;\phi}$ are calculated as

$$u^{t}{}_{;t} = \frac{1}{2}(g^{tt}g_{tt,r} + g^{t\phi}g_{t\phi,r})u^{r} - \frac{1}{2}g^{tr}(g_{tt,r} + g_{t\phi,r}\Omega)u^{t}, \tag{E3}$$

$$u^{r}{}_{;r} = \frac{du^{r}}{dr} + \frac{1}{2}g^{rr}g_{rr,r}u^{r} + (g^{tr}g_{tr,r} + g^{r\phi}g_{r\phi,r})u^{r} + \frac{1}{2}\left[g^{tr}(g_{tt,r} + g_{t\phi,r}\Omega) + g^{r\phi}(g_{t\phi,r} + g_{\phi\phi,r}\Omega)\right]u^{t}, \tag{E4}$$

$$u^{\theta}{}_{;\theta} = \frac{1}{2}g^{\theta\theta}g_{\theta\theta,r}u^{r}, \tag{E5}$$

$$u^{\phi}{}_{;\phi} = \frac{1}{2}(g^{t\phi}g_{t\phi,r} + g^{\phi\phi}g_{\phi\phi,r})u^{r} - \frac{1}{2}g^{r\phi}(g_{t\phi,r} + g_{\phi\phi,r}\Omega)u^{t}. \tag{E6}$$

Then, the expansion Θ is calculated by the form

$$\Theta = \frac{du^{r}}{dr} + \Theta_{r}, \tag{E7}$$

where Θ_{r} is defined as

$$\Theta_{r} = \frac{u^{r}}{2}\left(g^{tt}g_{tt,r} + g^{rr}g_{rr,r} + g^{\theta\theta}g_{\theta\theta,r} + g^{\phi\phi}g_{\phi\phi,r} + 2g^{tr}g_{tr,r} + 2g^{t\phi}g_{t\phi,r} + 2g^{r\phi}g_{r\phi,r}\right) \tag{E8}$$

We finally calculate the shear rate $\sigma_{(r)(\phi)}$ which can be calculated as $\sigma_{(r)(\phi)} = \sigma_{r} + \sigma_{u}(du^{r}/dr) + \sigma_{\ell}(d\ell/dr)$. By using the tetrads are given in Appendix C, the shear rate $\sigma_{(r)(\phi)}$ measured in the FRF is calculated by the shear rate $\sigma_{\mu\nu}$ measured in KSF as

$$\sigma_{(r)(\phi)} = e^{\mu}{}_{(r)}e^{\nu}{}_{(\phi)}\sigma_{\mu\nu} = \frac{1}{2}(u_{\mu;\nu} + u_{\nu;\mu})e^{\mu}{}_{(r)}e^{\nu}{}_{(\phi)} - \frac{\Theta}{3}e_{\mu}{}^{(r)}e^{\mu}{}_{(\phi)}. \tag{E9}$$

By substituting $u_{\mu;nu}$ given by Eq. (E1) into Eq. (E9), we can analytically calculate the coefficients σ_{r}, σ_{u} and σ_{ℓ}.

APPENDIX F: CALCULATIONS FOR ℓ_{*}

F1 Derivation of ℓ_{*} in Kerr-Schild coordinate

The explicit form for ℓ_{*} is obtained by the direct calculation of $\ell_{*}^{2} = r^{2}(\Gamma^{\mu}_{\theta\nu}u_{\mu}u^{\nu})_{1}$ where $(\Gamma^{\mu}_{\theta\nu}u_{\mu}u^{\nu})_{1}$ is calculated from $\Gamma^{\mu}_{\theta\nu}u_{\mu}u^{\nu}$ until the order of $\cos\theta$. $2\Gamma^{\mu}_{\theta\nu}u_{\mu}u^{\nu}$ is calculated as

$$2\Gamma^{\mu}_{\theta\nu}u_{\mu}u^{\nu} = g_{tt,\theta}(u^{t})^{2} + g_{rr,\theta}(u^{r})^{2} + g_{\phi,\theta}(u^{\phi})^{2} + +2g_{tr,\theta}u^{t}u^{r} + 2g_{t\phi,\theta}u^{t}u^{\phi} + 2g_{r\phi,\theta}u^{r}u^{\phi}, \tag{F1}$$

where the derivatives of the metric components with respect to θ are calculated until the order of $\cos\theta$ around the equatorial plane $\theta = \pi/2$ as

$$g_{tt,\theta} = g_{tr,\theta} = g_{rr,\theta} = \frac{2ma^{2}}{r^{3}}(2\cos\theta), \quad g_{t\phi,\theta} = -\frac{2ma}{r}\left(1 + \frac{a^{2}}{r^{2}}\right)(2\cos\theta),$$
$$g_{r\phi,\theta} = -a\left[1 + \frac{2m}{r}\left(1 + \frac{a^{2}}{r^{2}}\right)\right](2\cos\theta), \quad g_{\phi\phi,\theta} = r^{2}\left[1 + \frac{a^{2}}{r^{2}} + \frac{2ma^{2}}{r^{3}}\left(2 + \frac{a^{2}}{r^{2}}\right)\right](2\cos\theta), \tag{F2}$$

and u^{t}, u^{r} and u^{ϕ} are expressed by $\mathcal{E}$, ℓ and u_{r} as

$$u^{t} = \mathcal{E}\left(1 + \frac{2m}{r}\right) + \frac{2m}{r}u_{r}, \quad u^{r} = -\frac{2m}{r}\mathcal{E} + \frac{\Delta}{r^{2}}u_{r} + \frac{a}{r^{2}}\ell, \quad u^{\phi} = \frac{1}{r^{2}}(\ell + au_{r}). \tag{F3}$$

By substituting u^{t}, u^{r} and u^{ϕ} given by Eq. (F3), we obtain the equation including the term with $(u_{r})^{2}$ which is calculated from $u^{\mu}u_{\mu} = -1$ as

$$\frac{\Delta}{r^{2}}(u^{r})^{2} = \mathcal{E}\left(1 + \frac{2m}{r}\right) - \frac{\ell^{2}}{r^{2}} - 1 + 2u_{r}\left(\frac{2m}{r}\mathcal{E} - \frac{a}{r^{2}}\ell\right). \tag{F4}$$

From Eq. (F1) with Eqs. (F2), (F3) and (F4), we can finally obtain $(\Gamma^{\mu}_{\theta\nu}u_{\mu}u^{\nu})_{1}$ as

$$(\Gamma^{\mu}_{\theta\nu}u_{\mu}u^{\nu})_{1} = \frac{\ell^{2} - a^{2}(\mathcal{E}^{2} - 1)}{r^{2}}, \tag{F5}$$

where the coefficients of u_{r} become null.

As shown in Abramowicz, Lanza & Percival (1997), in the Boyer-Lindquist coordinate we obtain the same expression as Eq. (F5). This is because the specific energy $\mathcal{E}$ and the angular momentum ℓ have the same expression for both coordinate, i.e. $\mathcal{E}_{\rm BL} = \mathcal{E}_{\rm KS}$ and $\ell_{\rm BL} = \ell_{\rm KS}$, as shown by the transformations of four velocities given by Eq. (11). Here, "BL" and "KS" denote the physical quantities calculated by using the Boyer-Lindquist coordinate and the Kerr-Schild coordinate, respectively.

F2 Derivative of ℓ_* with respect to r

We express the derivative $d\ell_*/dr$ by the combination of du^r/dr and $d\ell/dr$ as

$$\frac{d\ell_*}{dr} = \ell_*^r + \ell_*^u \frac{du^r}{dr} + \ell_*^\ell \frac{d\ell}{dr}, \tag{F6}$$

where ℓ_*^r, ℓ_*^u and ℓ_*^ℓ are calculated as

$$\ell_*^r = -\frac{a^2\mathcal{E}}{\ell_*}\mathcal{E}_r, \quad \ell_*^u = -\frac{a^2\mathcal{E}}{\ell_*}\mathcal{E}_u, \quad \ell_*^\ell = -\frac{a^2\mathcal{E}}{\ell_*}\mathcal{E}_\ell + \frac{\ell}{\ell_*}. \tag{F7}$$

Here, $\mathcal{E}_r$, $\mathcal{E}_u$ and $\mathcal{E}_\ell$ are defined to have the relation $d\mathcal{E}/dr = \mathcal{E}_r + \mathcal{E}_u(du^r/dr) + \mathcal{E}_\ell(\ell/dr)$ and are calculated fully analytically or numerically.

This paper has been typeset from a TEX/ LATEX file prepared by the author.